STRUCTURES OF RESPIRATORY SYNCYTIAL VIRUS G ANTIGEN BOUND TO BROADLY NEUTRALIZING ANTIBODIES FOR VACCINE AND THERAPEUTIC DESIGN

A dissertation submitted in partial satisfaction of the requirements for the degree of

DOCTOR OF PHILOSOPHY

In

CHEMISTRY

By

Stanislav O. Fedechkin

December 2018

The Dissertation of Stanislav Fedechkin is approved:

_____
Professor Rebecca DuBois, chair

_____
Professor Michael Stone

_____
Professor Seth Rubin

_____
Lori G Kletzer Vice Provost and Dean of Graduate Studies

Table of Contents

List of Tables

List of Figures

Abstract

STRUCTURES OF RESPIRATORY SYNCYTIAL VIRUS G ANTIGEN BOUND TO BROADLY NEUTRALIZING ANTIBODIES FOR VACCINE AND THERAPEUTIC DESIGN

By Stanislav O. Fedechkin

Respiratory syncytial virus (RSV) is a top cause of severe lower respiratory tract disease and mortality in young children and the elderly. The viral envelope G glycoprotein contributes to pathogenesis through its roles in host cell attachment and modulation of host immunity. Although the G glycoprotein is a target of protective RSV-neutralizing antibodies, its development as a vaccine antigen has been hindered by its heterogeneous glycosylation and sequence variability outside a conserved central domain (CCD). We describe the cocrystal structures of three high-affinity broadly neutralizing human monoclonal antibodies bound to the RSV G CCD. All three antibodies bind to conformational epitopes that span a highly conserved and flexible surface, illuminating an important region of vulnerability. We further show that isolated RSV G CCD activates the chemokine receptor CX3CR1 and that antibodies block this activity. These studies provide a template for rational vaccine design targeting this key contributor to RSV disease.

Acknowledgments

Thank you Rebecca for all of your help and support! I appreciate the learning opportunity and the growing that took place with your guidance. I want to thank Michael Stone, Seth Rubin, Phil Berman and many more professors at UCSC who have provided valuable advice and helped guide me on my career path. I want to thank all of the members of the DuBois lab who've helped with work and supported me. I'd like to thank my family and friends for allowing me to explore my interests. I'd also like to thank the Department of Chemistry and Biochemistry at UC Santa Cruz for enabling me to be successful within the graduate program. I want to thank the Santa Cruz community for providing a safe and beautiful place for me to complete my Ph.D. studies.

RSV Field Overview

Starting at the end 2015, we began a collaboration with Trellis Biosciences in hopes of understanding the molecular basis for respiratory syncytial virus (RSV) neutralization by antibodies targeting the RSV G glycoprotein. Trellis developed a proprietary technique called CellSpot™ to screen B-cell repertoires from healthy donor individuals, sort for B-cells that target specific antigens, and sequence the B-cell antibodies, with the ultimate goal of developing therapeutic antibodies. One of the unique features of CellSpot™ is to isolate B cells directly from human blood, backed by the idea that humans can produce excellent affinity matured antibodies over the years of a lifetime, especially compared to standard immunization protocols which typically involve immunizing an animal over a short amount of time 8-12 weeks. In addition, CellSpot™ allows for the isolation of antibodies with multiple parameters, such as cross-reactivity and high affinity, with the antibodies derived from the healthy donor's immune system so they should have high safety as a therapeutic. Using CellSpot™, Trellis was able to isolate extremely tight binding antibodies (K_D=1-500 pM) that were also cross reactive for subtypes A and B of RSV (1). Trellis provided our lab with these antibody reagents and sequences.

The majority of the work done on RSV G was biological in nature, looking at the role of RSV G in cell attachment, immunity and immune modulation. There was virtually no structural information on G. It was well established that RSV G is one of the major immunogenic proteins on the RSV surface (Fig. A). At the start of the

project in 2016, there were virtually no effective and inexpensive treatments or preventatives for RSV. Palivizumab is an antibody prophylaxis used in infants to reduce morbidity, however it has limited use and target population due to its cost and delivery issues (2). Immunization to prevent RSV has long been a goal in the field, but challenges associated with immunizing infants (an ideal RSV vaccine would prevent disease in the first 6 month of life and give life long immunity) and creating a safe vaccine are still present. Specifically, there are major safety concerns for RSV vaccine, since a 1960's vaccine trials with formalin-inactivated RSV (FI-RSV) was associated with enhanced disease. Today, we have a clearer understanding of why FI-RSV failed (3). The F antigen conformation was altered to the less immunogenic and protective post-fusion form and no pre-fusion F was found on the surface (4). In addition, a number of studies have shown that the G antigen is associated with pathogenicity and can lead to severe immune response outcomes (eosinophilia) (5). Thus, the resulting immune response from FI-RSV vaccine produced a combination of low-affinity non-neutralizing antibodies and Th2-biased response.

As of 2016, there are over 19 RSV vaccine candidates and therapeutics in development, ranging from structure-based subunit vaccines, particle based, live-attenuated, nonreplicating and gene based vectors (6). In addition, the populations targeted have expanded to not only include immunization of infants and young children, but also immunization of pregnant women and older adults. The population which is at the highest risk of morbidity and severe disease outcomes for RSV is children <6 months of age. One approach to protect this population is through

immunizing pregnant women in hopes of producing and transferring maternal antibodies against RSV to the child. Maternal immunization has been gaining attention and several vaccines are in development.

Since 2013, there have also been advancements in structure-based vaccinology and the field had several proof-of-principle and first in class studies showing the feasibility of such approaches. One of the prominent areas of study in this field also involved RSV, focusing on the fusion protein. In one study stable scaffolds of the palivizumab epitope on F were generated and inserted into virus like particles (VLPs) (7). These and additional constructs were tested in animals and showed to induce neutralizing antibodies in rodents and macaques. Another study produced the full-length RSV fusion protein ectodomain stabilized through cysteines and hydrophobic cavity filling mutations (8). Immunization with this construct produced a protective immune response in mice and macaques. Another area of structure based-vaccinology is focused on Influenza A HA protein. Two approaches were made to design a structure-based vaccine: one using a headless HA and another using a conserved HA stem chimera with heterologous heads with the goal of producing a universal influenza vaccine (9, 10). Both approaches produced a modest protective immune response in animals eliciting strain-independent neutralizing antibodies. Overall, these studies set the precedent in the field that using structurally designed immunogens can offer protection and the potential for lasting immunity.

The RSV G sequence is highly variable and defines the RSV subgroups A and B. The G protein is heavily glycosylated with 30–40 O-linked glycans and 4–5 N-

linked glycans (~60-65% of the entire protein mass), RSV G contains two highly glycosylated mucin-like domains (a study on a closely related virus, Human metapneumovirus (HMPV) showed that HMPV G attachment protein mucin domains are highly glycosylated and intrinsically disordered by SEC-MALLS-RI and SAXS) (11, 12). The G protein is typically 80-100 kDa when expressed in immortalized cell lines or ~180 kDa form in primary human airway epithelial cells (13).

However there is a short, highly conserved sequence, which we later termed the Central Conserved Domain (CCD), spanning 48 residues that is devoid of glycosylation. The CCD contains 13 residues that are completely conserved in all RSV strains and a number of other highly conserved residues. The CCD contains a cysteine noose motif with 1–4, 2–3 disulfide connectivity that is believed to mediate attachment to cells during infection. Past the cysteine noose, on the C-terminus there is a heparin-binding domain (HBD) rich with lysines and positively charged residues that have been shown to be involved in binding to heparan sulfate proteoglycans and glycosaminoglycans (14-17). Studies using a peptide sequence of the HBD show that it inhibits RSV infection and binds to HEp-2 cells (18). However, there's been some debate in the field whether heparan sulfate proteoglycans are relevant to RSV infection, as it has been shown to be absent in primary cells, such as human airway epithelial cells, whereas many of the studies showing the importance of the HDB and heparan sulfate were performed in immortalized cell lines.

At the start of the project, we had linear epitope peptide mapping data showing where several of the Trellis anti-G monoclonal antibodies bound. A number

of the antibodies did not bind to linear peptides, raising the possibility that these antibodies are binding to non-linear and/or conformational epitopes within G. We initially hypothesized that all of the antibodies would bind to the CCD (although it may be possible that some antibodies bind to glycans, however the high degree of sequence variability and high degree of glycosylation variability makes this possibility unlikely). Our hypothesis was based on that the antibodies had all sub-nanomolar binding affinity and were cross-reactive across RSV strain A2 and B1. Thus, the antibodies were likely to bind to regions that had high sequence conservation and were accessible to antibodies, meaning regions outside the heavily glycosylated mucin-like regions, therefore the CCD.

Early on in the project, Trellis was considering moving forward with initiating a vaccine study using linear epitope peptide sequences of G (immunizing animals with short sequences of the CCD). At the time, it was widely believed that the G protein lacked defined structure or conformation outside of the two disulfides in the CCD. There were two minimal NMR structures solved in 1996 for bovine RSV G and another in 2002 for human RSV G (19, 20). These structures only showed ~19 residues of the CCD, mostly involving the two disulfides. By examining the sequence of the CCD, we noted that linear epitope peptide sequences preceded the cysteine noose regions, and we anticipated that antibodies would bind to additional regions of the CCD outside of the linear epitope. Likewise, we hypothesized that immunizing with just linear epitopes would be unlikely to elicit high affinity neutralizing antibodies.

Our goal was to define and determine the antibody epitopes on G for the Trellis antibody suite. We were also interested in determining the structure of larger CCD construct in order to investigate its conformational character. We were also interested in extending these studies to better understand the RSV attachment process and potential interactions with receptors. After optimizing mAb digestion procedure to isolate Fab and developing a co-purification method for isolating Fab complexes bound to RSV G, we were able to determine our first structure with 3D3 antibody bound to the CCD. Surprisingly, in the structure RSV G CCD has conformational character and the 3D3 antibody actually binds to a larger, three-dimensional epitope beyond that which was predicted by linear peptide mapping. Since then, 5 structures of RSV G bound to antibodies have been solved and all structures show conformational epitopes with G CCD (21, 22). In addition, a renewed focus on G as a vaccine candidate has been made with a number of studies investigating the effects of immunizing with the CCD. Currently, studies into receptor binding and immune modulation by RSV G are underway.

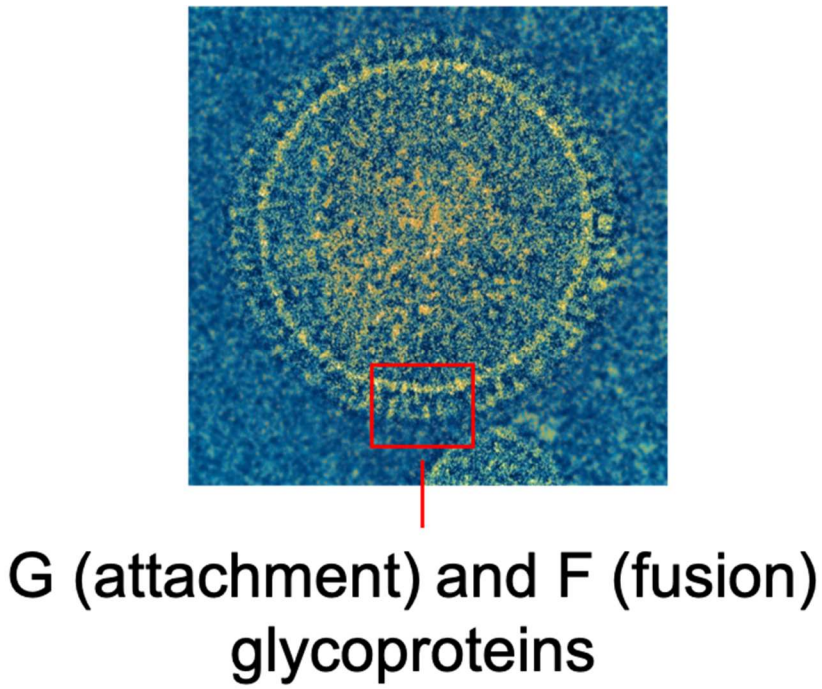

Fig. A. Respiratory syncytial virus glycoprotein electron microscope.

F and G glycoprotein are visible as projections on the surface. Courtesy of NIAID.

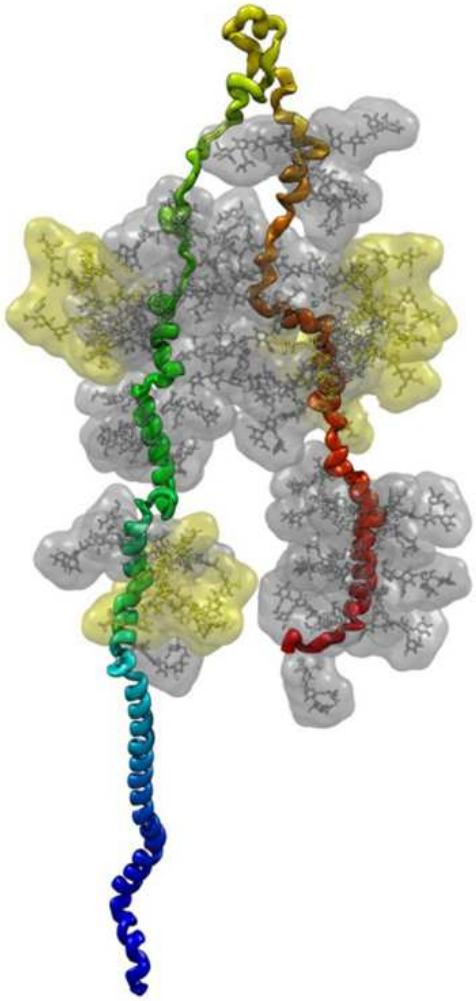

Fig. B. RSV G ectodomain model generated using steered molecular dynamics

(NAMD).

McLellan JS, Ray WC, Peeples ME. Structure and function of respiratory syncytial virus surface glycoproteins. Curr Top Microbiol Immunol. 2013;372:83-104.

References

1. Collarini EJ, Lee FE, Foord O, Park M, Sperinde G, Wu H, Harriman WD, Carroll SF, Ellsworth SL, Anderson LJ, Tripp RA, Walsh EE, Keyt BA, Kauvar LM. 2009. Potent high-affinity antibodies for treatment and prophylaxis of respiratory syncytial virus derived from B cells of infected patients. J Immunol 183:6338-6345.
2. Anonymous. 1998. Palivizumab, a Humanized Respiratory Syncytial Virus Monoclonal Antibody, Reduces Hospitalization From Respiratory Syncytial Virus Infection in High-risk Infants. Pediatrics 102:531-537.
3. Acosta PL, Caballero MT, Polack FP. 2015. Brief History and Characterization of Enhanced Respiratory Syncytial Virus Disease. Clin Vaccine Immunol 23:189-195.
4. Killikelly AM, Kanekiyo M, Graham BS. 2016. Pre-fusion F is absent on the surface of formalin-inactivated respiratory syncytial virus. Scientific Reports 6.
5. Haynes LM, Jones LP, Barskey A, Anderson LJ, Tripp RA. 2003. Enhanced disease and pulmonary eosinophilia associated with formalin-inactivated respiratory syncytial virus vaccination are linked to G glycoprotein CX3C-CX3CR1 interaction and expression of substance P. J Virol 77:9831-9844.
6. Mazur NI, Higgins D, Nunes MC, Melero JA, Langedijk AC, Horsley N, Buchholz UJ, Openshaw PJ, McLellan JS, Englund JA, Mejias A, Karron RA,

Simoes EA, Knezevic I, Ramilo O, Piedra PA, Chu HY, Falsey AR, Nair H, Kragten-Tabatabaie L, Greenough A, Baraldi E, Papadopoulos NG, Vekemans J, Polack FP, Powell M, Satav A, Walsh EE, Stein RT, Graham BS, Bont LJ, Respiratory Syncytial Virus Network F. 2018. The respiratory syncytial virus vaccine landscape: lessons from the graveyard and promising candidates. Lancet Infect Dis 18:e295-e311.

7. Schickli JH, Whitacre DC, Tang RS, Kaur J, Lawlor H, Peters CJ, Jones JE, Peterson DL, McCarthy MP, Van Nest G, Milich DR. 2015. Palivizumab epitope-displaying virus-like particles protect rodents from RSV challenge. J Clin Invest 125:1637-1647.

8. McLellan JS, Chen M, Joyce MG, Sastry M, Stewart-Jones GB, Yang Y, Zhang B, Chen L, Srivatsan S, Zheng A, Zhou T, Graepel KW, Kumar A, Moin S, Boyington JC, Chuang GY, Soto C, Baxa U, Bakker AQ, Spits H, Beaumont T, Zheng Z, Xia N, Ko SY, Todd JP, Rao S, Graham BS, Kwong PD. 2013. Structure-based design of a fusion glycoprotein vaccine for respiratory syncytial virus. Science 342:592-598.

9. Hai R, Krammer F, Tan GS, Pica N, Eggink D, Maamary J, Margine I, Albrecht RA, Palese P. 2012. Influenza viruses expressing chimeric hemagglutinins: globular head and stalk domains derived from different subtypes. J Virol 86:5774-5781.

10. Impagliazzo A, Milder F, Kuipers H, Wagner MV, Zhu X, Hoffman RM, van Meersbergen R, Huizingh J, Wanningen P, Verspuij J, de Man M, Ding Z,

Apetri A, Kukrer B, Sneekes-Vriese E, Tomkiewicz D, Laursen NS, Lee PS, Zakrzewska A, Dekking L, Tolboom J, Tettero L, van Meerten S, Yu W, Koudstaal W, Goudsmit J, Ward AB, Meijberg W, Wilson IA, Radosevic K. 2015. A stable trimeric influenza hemagglutinin stem as a broadly protective immunogen. Science 349:1301-1306.

11. McLellan JS, Ray WC, Peeples ME. 2013. Structure and function of respiratory syncytial virus surface glycoproteins. Curr Top Microbiol Immunol 372:83-104.

12. Leyrat C, Paesen GC, Charleston J, Renner M, Grimes JM. 2014. Structural Insights into the Human Metapneumovirus Glycoprotein Ectodomain. Journal of Virology 88:11611-11616.

13. Kwilas S, Liesman RM, Zhang L, Walsh E, Pickles RJ, Peeples ME. 2009. Respiratory syncytial virus grown in Vero cells contains a truncated attachment protein that alters its infectivity and dependence on glycosaminoglycans. J Virol 83:10710-10718.

14. Shields B, Mills J, Ghildyal R, Gooley P, Meanger J. 2003. Multiple heparin binding domains of respiratory syncytial virus G mediate binding to mammalian cells. Arch Virol 148:1987-2003.

15. Hallak LK, Collins PL, Knudson W, Peeples ME. 2000. Iduronic acid-containing glycosaminoglycans on target cells are required for efficient respiratory syncytial virus infection. Virology 271:264-275.

16. Feldman SA, Hendry RM, Beeler JA. 1999. Identification of a linear heparin binding domain for human respiratory syncytial virus attachment glycoprotein G. J Virol 73:6610-6617.

17. Krusat T, Streckert HJ. 1997. Heparin-dependent attachment of respiratory syncytial virus (RSV) to host cells. Arch Virol 142:1247-1254.

18. Donalisio M, Rusnati M, Cagno V, Civra A, Bugatti A, Giuliani A, Pirri G, Volante M, Papotti M, Landolfo S, Lembo D. 2012. Inhibition of Human Respiratory Syncytial Virus Infectivity by a Dendrimeric Heparan Sulfate-Binding Peptide. Antimicrobial Agents and Chemotherapy 56:5278-5288.

19. Doreleijers JF, Langedijk JP, Hard K, Boelens R, Rullmann JA, Schaaper WM, van Oirschot JT, Kaptein R. 1996. Solution structure of the immunodominant region of protein G of bovine respiratory syncytial virus. Biochemistry 35:14684-14688.

20. Sugawara M, Czaplicki J, Ferrage J, Haeuw JF, Power UF, Corvaia N, Nguyen T, Beck A, Milton A. 2002. Structure-antigenicity relationship studies of the central conserved region of human respiratory syncytial virus protein G. J Pept Res 60:271-282.

21. Fedechkin SO, George NL, Wolff JT, Kauvar LM, DuBois RM. 2018. Structures of Respiratory Syncytial Virus G Antigen Bound to Broadly-Neutralizing Antibodies. Science Immunology In press.

22. Jones HG, Ritschel T, Pascual G, Brakenhoff JPJ, Keogh E, Furmanova-Hollenstein P, Lanckacker E, Wadia JS, Gilman MSA, Williamson RA,

Roymans D, van 't Wout AB, Langedijk JP, McLellan JS. 2018. Structural basis for recognition of the central conserved region of RSV G by neutralizing human antibodies. PLoS Pathog 14:e1006935.

Chapter I:

Structures of respiratory syncytial virus G antigen bound to broadly neutralizing antibodies.

INTRODUCTION

Respiratory syncytial virus (RSV) infects most children by age 2 and is the leading cause of severe lower respiratory tract disease in children worldwide (1–4). RSV is a major cause of mortality, with an estimated 118,000 deaths per year in children under age 5 (3, 5). RSV is also a major cause of morbidity in the elderly and immunocompromised populations. No licensed RSV vaccine exists, and the only widely used intervention is palivizumab (Synagis), a monoclonal antibody (mAb) against the RSV F glycoprotein that reduces disease severity in premature birth infants (6). RSV F is required for infectivity, is less variable overall than RSV G, and is the target of most neutralizing antibodies (7). However, the recent failures of two prominent RSV F vaccines, a phase 3 clinical trial in older adults (Novavax) and a phase 2b trial in older adults (MedImmune), highlight the urgent need for new approaches. Because these vaccines contained RSV F immunogen in its postfusion conformation, one emerging approach is focused on the generation of RSV F immunogens that are stabilized in the prefusion conformation, as revealed by x-ray crystallographic studies (8). In addition, RSV G is increasingly recognized as a

critical target (9), yet its development as a vaccine antigen has been hindered by its dense and heterogeneous N- and O-glycosylation in the highly variable mucin-like regions and a paucity of information correlating specific molecular structure with biological activity.

Although variable overall, RSV G (298 residues) contains a ~40–amino acid central conserved domain (CCD) that is devoid of glycosylation and plays key roles in both virus infection and viral pathogenesis (Fig. 1). Specifically, RSV G CCD contains a CX3C chemokine motif that facilitates binding to the human chemokine receptor CX3CR1, a critical step for RSV infection in human airway epithelial cells (10–13). Notably, a soluble form of RSV G is secreted from infected cells beginning ~6 hours after infection, long before the appearance of RSV virions at 12 hours (14, 15). In vivo, this soluble G protein competes with the natural ligand CX3CL1 (also known as fractalkine) for binding to CX3CR1, modulating signaling and trafficking of CX3CR1+ immune cells, contributing to airway congestion (13, 16–18). RSV with the G gene deleted is highly attenuated in vivo (19). Moreover, RSV with an insertion in the CX3C motif of G (CX4C) that prevents CX3CR1 binding has markedly reduced disease severity in vivo (20). In a recent study, elevated concentrations of both anti-G and anti–prefusion-F antibodies were associated with lower clinical disease severity scores, despite the substantially lower absolute abundance of anti-G antibodies compared to anti-F antibodies (7). These results strongly support a renewed focus on RSV G as a target in vaccine and therapeutic antibody development.

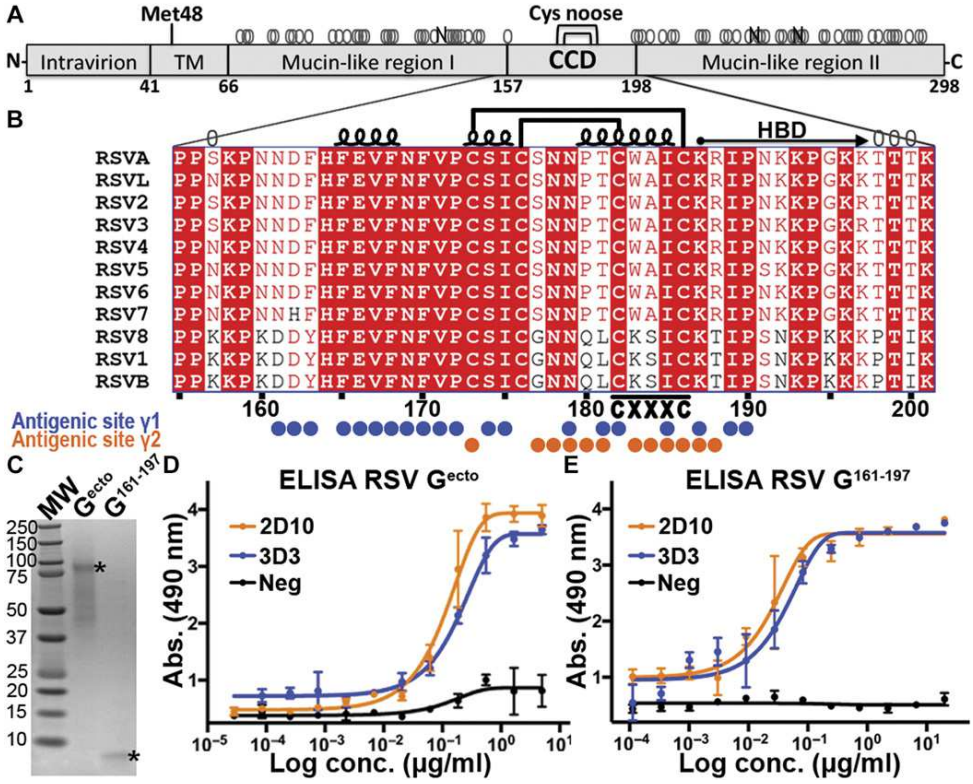

Fig. 1.1. bnmAbs 3D3 and 2D10 bind RSV $G^{161\text{-}197}$.

(A) Schematic of the RSV G glycoprotein from RSV strain A2, including the transmembrane region (TM), central conserved region (CCD), and the cysteine noose (Cys noose). Met48 is the alternate initiation site for the production of soluble RSV G. Predicted N- and O-linked glycans are shown by black "N" and gray "O," respectively. (B) Sequence alignment of RSV G CCD from diverse RSV strains. Amino acids 157 and 198 are predicted to be O-glycosylated in RSV strain A2 (gray "O") and represent the boundaries. Secondary structure, disulfide bonds, and heparin binding domain (HBD) are displayed. Amino acids within bnmAb 3D3 and 2D10 epitopes (antigenic sites γ1 and γ2) are labeled with blue and orange circles, respectively. (C) Coomassie-stained SDS-PAGE of RSV G^{ecto} and RSV $G^{161\text{-}197}$. (D) ELISA showing binding of bnmAbs 3D3 and 2D10 to RSV G^{ecto}. (E) ELISA showing binding of bnmAbs 3D3 and 2D10 to RSV $G^{161\text{-}197}$. ELISA experiments were performed in biological triplicates.

RESULTS

Conformational antigenic site γ1

We first investigated bnmAb 3D3, a native human antibody which binds RSV G with high affinity [Kd (dissociation constant)= 1.1 pM], shows broadly neutralizing activity across nearly all circulating strains and is in development as a post-infection therapeutic (22, 29). Purified antigen-binding fragment (Fab) 3D3 formed stable complexes with its linear epitope peptide (RSV $G^{162-172}$) in solution (fig. S1), and we determined the crystal structure of the Fab 3D3-RSV $G^{162-172}$ complex to 2.40 Å resolution (Fig. 2A, fig. S2, and table S1). The RSV $G^{162-172}$ peptide contains a short helix and projects several hydrophobic residues, including Phe163, Phe165, Phe168, Phe170, and Pro172, into a ~700 Å2 groove formed by heavy-chain complementarity-determining regions (CDRs) 1, 2, and 3 and light-chain CDRs 1 and 3. Surprisingly, the distal six amino acids of the extended heavy-chain CDR3 formed no molecular contacts with the linear epitope peptide (Fig. 2A), indicative of a larger epitope.

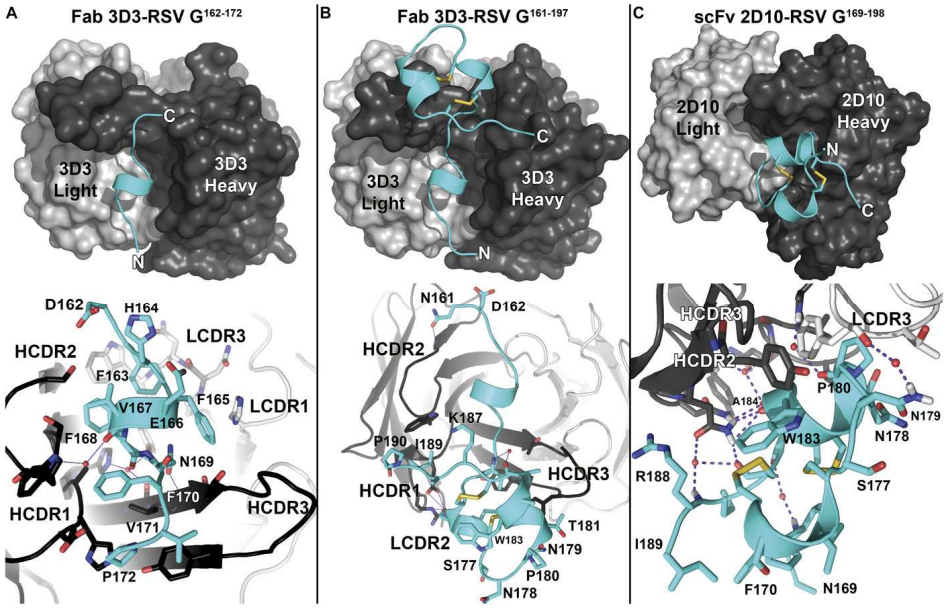

Fig. 1.2. Crystal structures of RSV G-antibody complexes.

Overall view (top) and zoom-in view (bottom) of the (A) Fab 3D3-RSV $G^{162-172}$complex, (B) Fab 3D3-RSV $G^{161-197}$ complex, and (C) the scFv 2D10-RSV $G^{169-198}$complex. In all panels, RSV G is colored cyan, bnmAb heavy chain is colored dark gray, and bnmAb light chain is colored light gray. Water molecules are shown in red. Hydrogen bonds are shown as dashes. Heavy-chain CDRs (HCDR1-3) and light-chain CDRs (LCDR1-3) are labeled.

To examine whether bnmAb 3D3 interacts with a larger RSV G epitope, we produced in Escherichia coli a recombinant fragment of RSV G (strain A2) that includes the 3D3 linear epitope sequence and the following 25 amino acids spanning the CX3C chemokine motif (RSV G161-197). Antibody 3D3 binds to recombinant RSV G161-197 similarly to recombinant RSV G ectodomain (RSV Gecto) (strain A2) and forms a stable complex in solution (Fig. 1 and fig. S1). We determined the crystal structure of the Fab 3D3-RSV G161-197 complex to 2.40 Å resolution (Fig. 2B, fig. S2, and table S1). The structure reveals additional interactions between bnmAb 3D3 and RSV G residues beyond the linear epitope, increasing the binding interface to ~1060 Å2. Specifically, heavy-chain CDR3 interacts with the RSV G cysteine noose (residues 173 to 186), which contains four cysteine residues in nested disulfide bonds (1-4 and 2-3), as observed previously in nuclear magnetic resonance structures of this ~15-residue region (fig. S2) (30, 31). Additional interactions were observed between heavy-chain CDRs 1 and 2 and RSV G residues 189 and 190. Together, we find that the high-affinity and protective bnmAb 3D3 binds to RSV G at a discontinuous conformational epitope, which we have named antigenic site γ1.

Conformational antigenic site γ2

We next investigated bnmAb 2D10, which also binds RSV G but whose epitope could not be characterized by linear epitope mapping (22, 29). We found that bnmAb 2D10 binds to recombinant RSV $G^{161-197}$ similarly to recombinant RSV Gecto (Fig. 1), revealing that its epitope is also within the conserved, unglycosylated

region of RSV G. We then engineered a recombinant 2D10 single-chain variable fragment (scFv), which forms stable complexes with a synthetic RSV G peptide (RSV $G^{169-198}$) in solution (fig. S1), and we determined the crystal structure of the scFv 2D10-RSV $G^{169-198}$ complex to 1.56 Å resolution (Fig. 2C, fig. S2, and table S1). Antibody 2D10 uses a twisted heavy-chain CDR3, heavy-chain CDR2, and light-chain CDR3 to bind to a ~550 $Å^2$epitope on the RSV G cysteine noose. The CX3C chemokine motif, which forms a short helix in the cysteine noose, is buried by bnmAb 2D10 binding. Although the 2D10 epitope is mostly continuous, composed mainly of residues 177 to 188, the two cysteines within the epitope form two disulfide bonds that induce strong conformational character to this epitope, which we have named antigenic site γ2.

Functional significance of antigenic sites γ1 and γ2

To understand the mechanism of virus neutralization and protection from disease by bnmAbs 3D3 and 2D10, we examined whether they inhibit RSV G modulation of $CX3CR1^+$ cells in an in vitro chemotaxis assay (Fig. 3A). First, we tested recombinant RSV G^{ecto} and found that it induces chemotaxis of human monocyte THP-1 cells, consistent with previous studies (13, 23). To determine if the RSV G CCD alone is sufficient to induce chemotaxis, we tested recombinant RSV $G^{161-197}$ and found that it induces chemotaxis at levels equivalent to RSV G^{ecto}. Preincubation of RSV $G^{161-197}$ with bnmAbs 3D3 and 2D10 markedly inhibited RSV $G^{161-197}$–induced chemotaxis, suggesting that the bnmAbs 3D3 and 2D10 block a

CX3CR1-binding site on RSV G. Control experiments show that the bnmAbs have no effect on chemotaxis induced by human CX3CL1, confirming the specificity of the bnmAbs (Fig. 3B). Last, to confirm that chemotaxis migration is induced by interactions with CX3CR1, we preincubated THP-1 cells with anti-CX3CR1 polyclonal antibodies, which significantly inhibited RSV $G^{161\text{-}197}$–induced chemotaxis (Fig. 3A) and CX3CL1-induced chemotaxis (Fig. 3B). Together, these studies establish that the 37–amino acid fragment RSV $G^{161\text{-}197}$ is sufficient to modulate CX3CR1 and that bnmAbs 3D3 and 2D10 specifically block this activity.

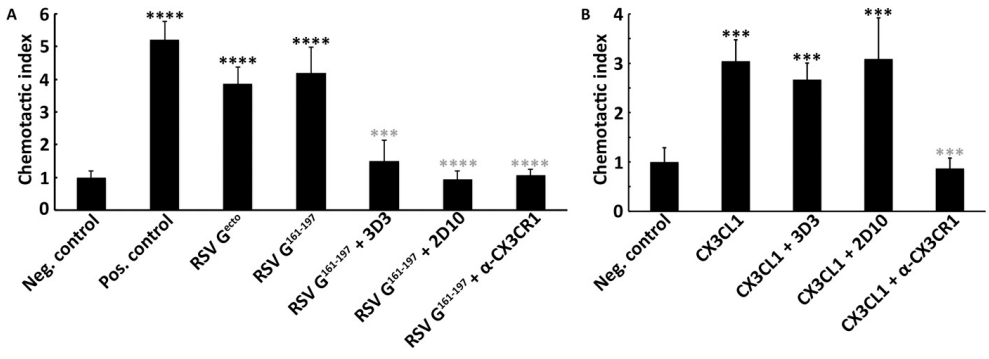

Fig. 1.3 bnmAbs 3D3 and 2D10 specifically block RSV G161-197–induced

chemotaxis.

Chemotaxis assays were performed in a Transwell plate, with THP-1 cells added to the upper chamber and chemoattractant added to the lower chamber. (A) Serum-free media were used as negative control, 10% FBS as positive control, 5 nM RSV G^{ecto}, or 5 nM RSV $G^{161\text{-}197}$. (B) Serum-free media containing BSA (1 mg/ml) were used as a negative control and 10 nM CX3CL1 (fractalkine) as a positive control. Chemotactic indices were determined by comparing the fold increase in cell migration toward the chemoattractant compared to cell migration toward serum-free media alone. Studies with bnmAbs (25 nM) were used to examine inhibition of RSV $G^{161\text{-}197}$–induced and CX3CL1-induced chemotaxis. Studies with anti-CX3CR1 preincubated with THP-1 cells in the upper chamber were used to examine antagonism of cell migration toward RSV $G^{161\text{-}197}$ and CX3CL1 in the lower chamber. Student's t test was performed. Black asterisks denote significance compared to negative control and gray asterisks denote significance compared to RSV $G^{161\text{-}197}$ (A) or CX3CL1 (B); ***$P < 0.001$, ****$P < 0.0001$. Chemotaxis experiments were performed in four biological replicates. Error bars indicate SEM.

Sequence conservation at antigenic sites γ1 and γ2

Last, to understand the molecular basis for RSV G activation of CX3CR1, we aligned diverse RSV G sequences and mapped conservation level onto the RSV G structure (Figs. 1B and 4A). Despite the overall high variability of full-length RSV G (53% identity between subtypes RSV A and B), the 37–amino acid fragment RSV $G^{161\text{-}197}$ that activates CX3CR1 contains 24 invariant residues (70% identity between subtypes RSV A and B). Notably, in the CX3C motif, only one of the three "X" amino acids, Ile185, is highly conserved, suggesting that this motif alone does not compose the CX3CR1-binding site (Fig. 4A). Rather, we find that the invariant cysteines in the CX3C motif stabilize a three-dimensional surface of highly conserved amino acids that form extensive atomic interactions across the entire region (Fig. 4B), consistent with bnmAb epitopes (Fig. 4A). Thus, the RSV G CCD forms a highly conserved three-dimensional surface poised for CX3CR1 binding (Fig. 4C and fig. S3). We note that the heparin-binding domain, which is immediately C-terminal to the cysteine noose, includes several conserved positively charged amino acids (Fig. 1B) (32). Whereas RSV does not use heparan sulfate proteoglycans (HSPGs) to infect human airway epithelial cells, RSV may use HSPGs to infect other cell types, as observed for RSV infection in immortalized cells (10). HSPGs may also play a role in binding of soluble RSV G to other human cells (33). We observed no structural or

sequence similarities between RSV G and CX3CL1, the only known ligand for CX3CR1, besides the presence of a CX3C motif and its two disulfide bonds (fig. S4). This structural divergence despite similar functionality suggests an opportunity to selectively develop therapies blocking interaction between the RSV G CCR and CX3CR1, a strategy that led to the development of the HIV entry inhibitor Maraviroc, an antagonist of the HIV co-receptor CCR5 (34).

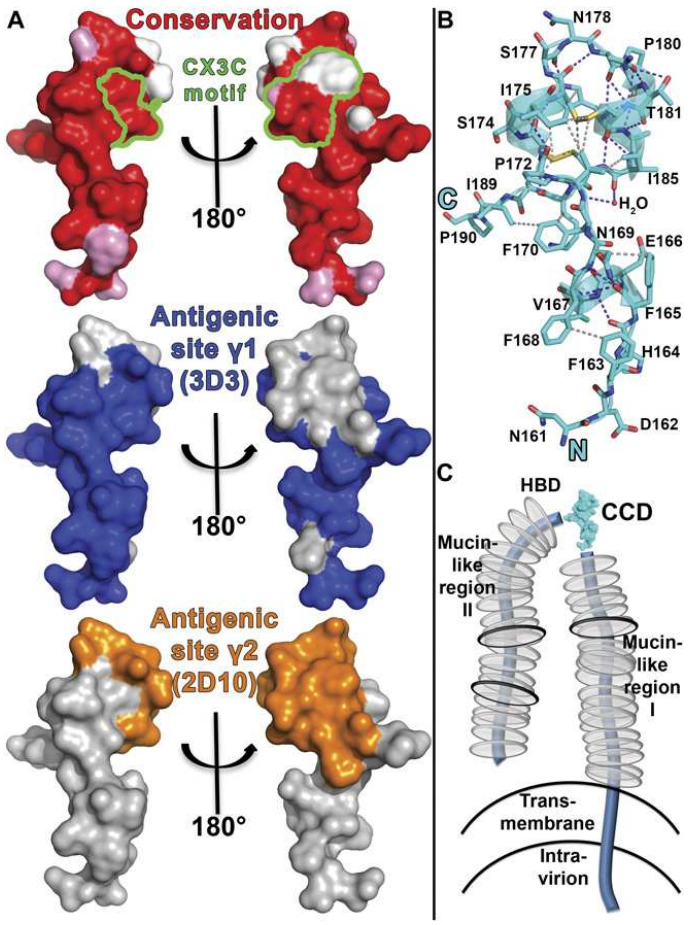

Fig. 1.4 Sequence conservation within antigenic sites γ1 and γ2, atomic interactions within the RSV G CCD, and model of RSV G glycoprotein.

A) Top: Surface representation of RSV G with amino acids colored according to conservation. Atoms from the main chain and conserved side chains are red, similar side chains are pink, and nonconserved side chains are white. The five CX3C motif amino acids are outlined in green. Middle and bottom: The epitope footprints of antigenic site γ1 (bnmAb 3D3 epitope) and antigenic site γ2 (bnmAb 2D10 epitope), respectively. (B) Structure of RSV $G^{161-197}$ with hydrogen bonds shown in purple dashes and representative side chain–side chain hydrophobic interactions (≤4.0 Å) shown in gray dashes. (C) Schematic of membrane-bound RSV G. N- and O-linked glycans are shown by black and gray discs, respectively.

DISCUSSION

Our studies define RSV G amino acids 161 to 197 as a key region of vulnerability that is accessible to antibody binding. Nearly half of RSV-specific human memory B cells target the G glycoprotein (24), and more than half of the anti-G antibodies in human serum target specifically the RSV G CCD (35). Consistent with these studies, 17 of 21 isolated human anti-G mAbs have linear epitopes that map to this region (fig. S5) (22, 24). Of the other four mAbs, we show that one (2D10) binds to an epitope adjacent to the epitope for 3D3 but largely nonoverlapping with it. A limitation of the present study is that definition of the epitopes for other mAbs has not yet been achieved nor have the epitopes been defined for bioactive anti-G mAbs that are strain-specific.

Overall, bnmAbs against this region of vulnerability exhibit high affinities and strain independence, neutralize RSV infection of human airway epithelial cells, inhibit soluble RSV G modulation of $CX3CR1^{+}$ cells, and decrease pathogenesis in animal models, supporting their development as therapeutic agents to prevent and treat RSV infection. To address global needs, a vaccine may be a more cost-effective intervention, with the present studies providing a firm foundation for constructing an immunogen that induces protective broadly neutralizing antibodies targeting the RSV G CCD. To avoid side effects, such an immunogen should not itself activate CX3CR1, a limitation whose feasibility awaits further study.

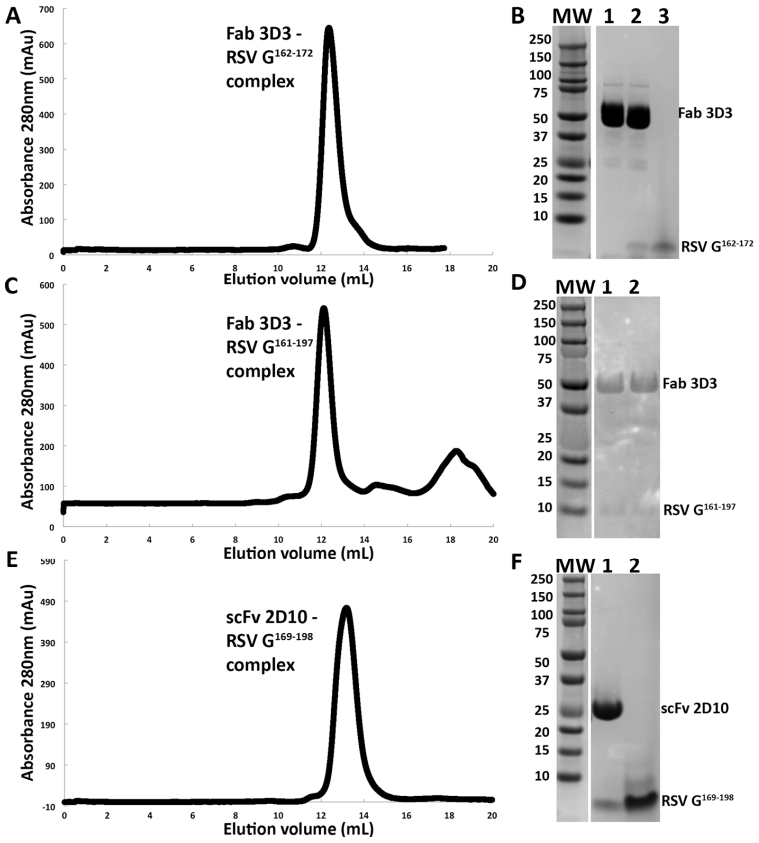

Fig. S1. Co-elution of RSV G-antibody complexes in solution.

(A, C, E) Superdex 200 size-exclusion chromatography purification traces of antibody-RSV G complexes. (B) Non-reducing SDS-PAGE of molecular weight markers in kD (MW), Fab 3D3 alone (lane 1), co-eluted Fab 3D3-RSV $G^{162-172}$ complex (lane 2), and RSV $G^{162-172}$ alone (lane 3). (D) Non-reducing SDS-PAGE of molecular weight markers in kD (MW) and co-eluted Fab 3D3-RSV $G^{161-197}$ complex (lanes 1 and 2). (F) Reducing SDS-PAGE of molecular weight markers in kD (MW), co-eluted scFv 2D10-RSV $G^{169-198}$ complex (lane 1), and RSV $G^{169-198}$ alone (lane 2).

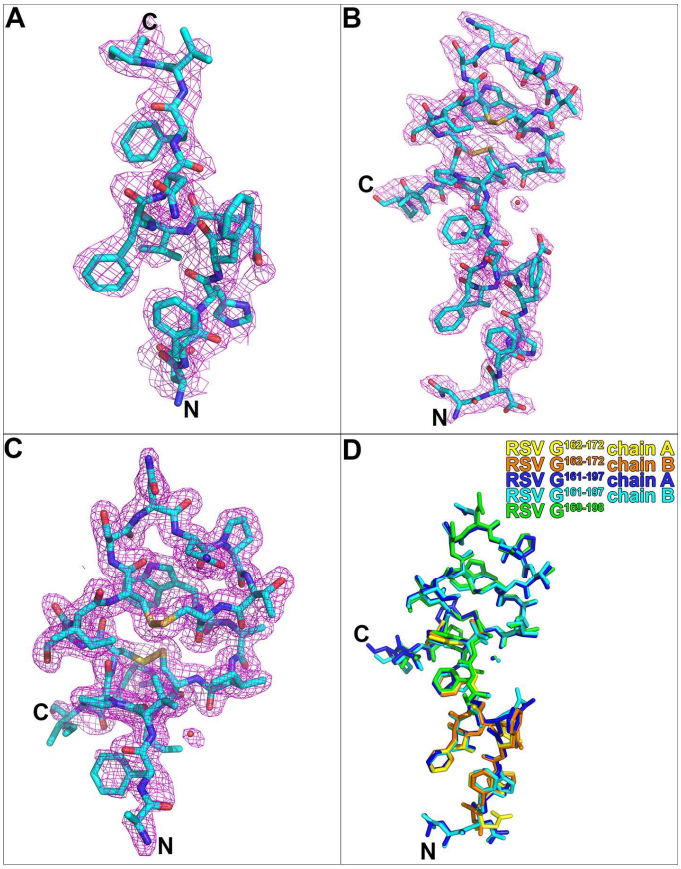

Fig. S2. Electron density maps (2Fo-Fc) for RSV G bound to antibodies.

(A) RSV $G^{162-172}$ when bound to Fab 3D3, (B) RSV $G^{161-197}$ when bound to Fab 3D3. (C) RSV $G^{169-198}$ when bound to scFv 2D10. In all cases, the electron density maps (2Fo-Fc) around RSV G are contoured at 1.0 σ. (D) Structural alignment of RSV G from all three structures. Note that in the Fab 3D3-RSV $G^{162-172}$ complex and Fab 3D3-RSV $G^{161-197}$ complex structures, there are two molecules of RSV G in the asymmetric units.

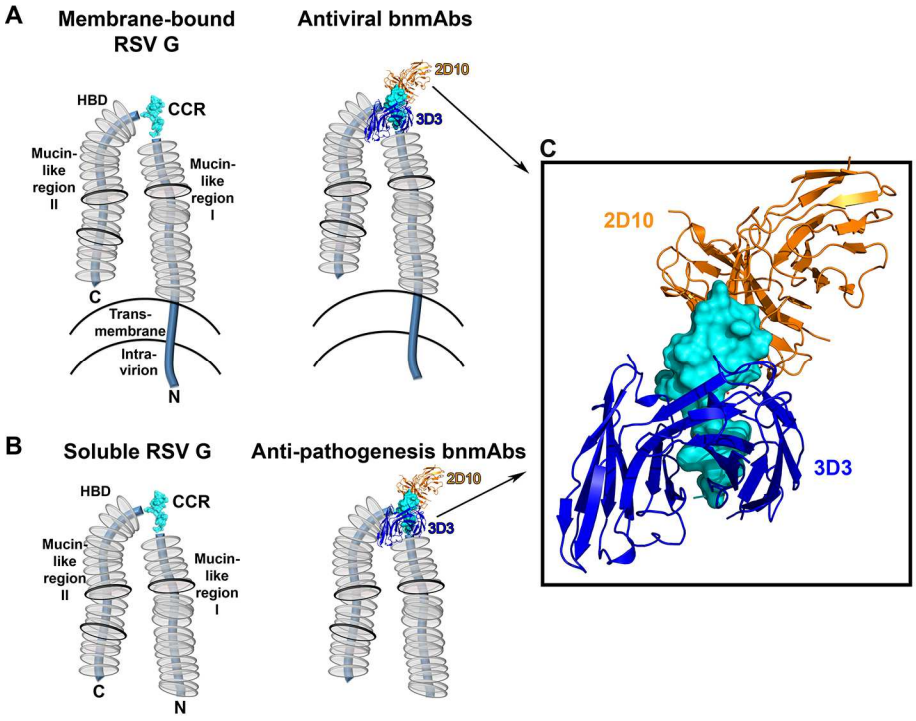

Fig. S3. Schematic of RSV G interactions with anti-G antibodies.

(A) Model of membrane-bound G glycoprotein on the surface of the RSV virion or the surface of RSV-infected cells alone (left) or bound by bnmAbs 3D3 and 2D10 (right). **(B)** Model of soluble RSV G glycoprotein, which is secreted from RSV-infected cells and modulates $CX3CR1^{+}$ immune cells, alone (left) or bound by bnmAbs 3D3 and 2D10 (right). **(C)** Zoom-in of RSV G CCR bound by bnmAbs 3D3 and 2D10. For clarity, only the variable regions of the bnmAbs are shown.

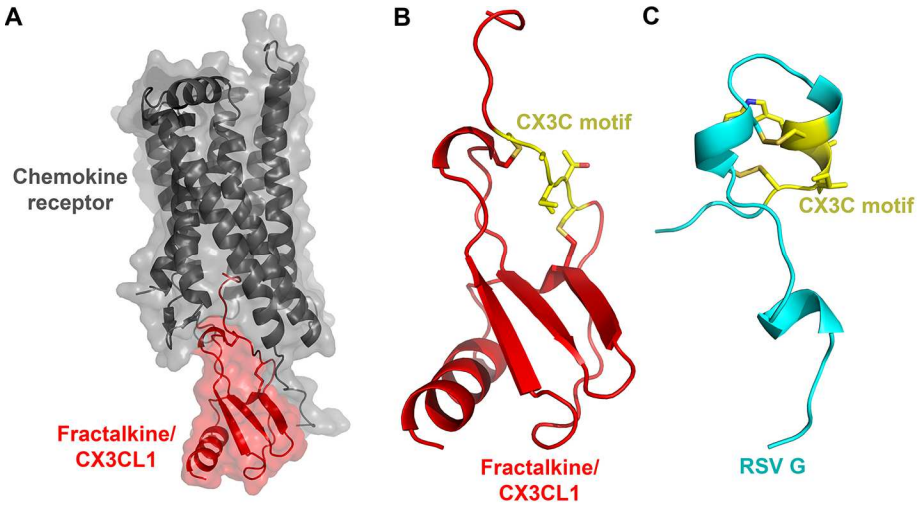

Fig. S4. Structural comparison of RSV G with fractalkine/CX3CL1.

(A) Structure of fractalkine/CX3CL1 (red) bound to the human cytomegalovirus G-protein coupled receptor US28 (grey) (PDB code 4XT1). US28 has 38% sequence identity with the human chemokine receptor CX3CR1. **(B)** Structure of fractalkine/CX3CL1 (red), in the same orientation as in panel a, with the amino acid side chains of the CX3C motif shown as sticks and colored yellow. **(C)** Structure of RSV $G^{161-197}$ (cyan)**,** with the amino acid side chains of the CX3C motif shown as sticks and colored yellow.

A

```
RSV G161-197  NDFHFEVFNFVPCSICSNNPTCWAICKRIPNKKPGK
RSVA          NDFHFEVFNFVPCSICSNNPTCWAICKRIPNKKPGK
RSVL          NDFHFEVFNFVPCSICSNNPTCWAICKRIPNKKPGK
RSV2          NDFHFEVFNFVPCSICSNNPTCWAICKRIPNKKPGK
RSV3          NDFHFEVFNFVPCSICSNNPTCWAICKRIPNKKPGK
RSV4          NDFHFEVFNFVPCSICSNNPTCWAICKRIPNKKPGK
RSV5          NDFHFEVFNFVPCSICSNNPTCWAICKRIPSKKPGK
RSV6          NDFHFEVFNFVPCSICSNNPTCWAICKRIPNKKPGK
RSV7          NHFHFEVFNFVPCSICSNNPTCWAICKRIPNKKPGK
RSV8          DDYHFEVFNFVPCSICGNNQLCKSICKTIPSNKPKK
RSV1          DDYHFEVFNFVPCSICGNNQLCKSICKTIPSNKPKK
RSVB          DDYHFEVFNFVPCSICGNNQLCKSICKTIPSNKPKK
              :.:*************.**  * :*** **.:** *
```

B

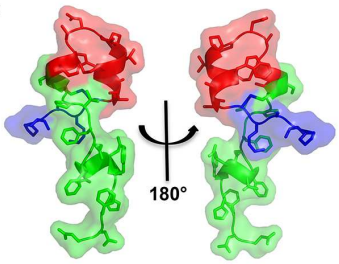

C

mAb	Linear Epitope[a]	Linear Epitope Sequence	Conformational Epitope Sequence[b]	Strain(s) Specificity	Reference[c]
3D3	164-172	----HFEVFNFVP--	NDF-FEVFNFVP-SI--N-TC--I-K-IP	RSV A, B	Collarini et al. 2009
2B11	162-172	--DFHFEVFNFVP--		RSV A, B	Collarini et al. 2009
1G8	164-172	----HFEVFNFVP--		RSV A, B	Collarini et al. 2009
10C6	165-169	-----FEVFN-----		RSV A, B	Collarini et al. 2009
1D4	165-171	-----FEVFNFV---		RSV A, B	Collarini et al. 2009
3G12	167-176	-------VFNFVPCSIC		RSV A, B	Collarini et al. 2009
1F12	166-172	------EVFNFVP--		RSV A, B	Collarini et al. 2009
1A5	161-170	-NDFHFEVFNF----		RSV A, B	Collarini et al. 2009
5D8	160-169	NNDFHFEVFN-----		RSV A, B	Collarini et al. 2009
2D10	N.D.	N.D.	C---SNNPT-WAICKR	RSV A, B	Collarini et al. 2009
1G1	N.D.	N.D.		RSV A, B	Collarini et al. 2009
6A12	N.D.	N.D.		RSV A, B	Collarini et al. 2009
AT34	161-170	-NDFHFEVFNF----		RSV A, B	Cortjens et al. 2017
AT40	162-170	--DFHFEVFNF----		RSV A, B	Cortjens et al. 2017
AT64G	162-170	--DFHFEVFNF----		RSV A, B	Cortjens et al. 2017
AT50	175-184	-ICSNNPTCWA-		RSV A	Cortjens et al. 2017
AT51	174-184	SICSNNPTCWA-		RSV A	Cortjens et al. 2017
AT61G	174-184	SICSNNPTCWA-		RSV A	Cortjens et al. 2017
AT32	185-193	ICKRIPNKK---		RSV A	Cortjens et al. 2017
AT33	186-193	-CKRIPNKK---		RSV A	Cortjens et al. 2017
AT42	N.D.	N.D.		RSV A, B	Cortjens et al. 2017

[a] Linear epitope sequence numbering in RSV strain A2. N.D. refers to no detectable binding to linear RSV G peptides.
[b] Conformational epitope sequences were determined in this study.
[c] References for linear epitope sequence mapping.

Fig. S5. Isolated human anti-G mAbs and epitope characterization.

(A) Sequence alignment of RSV G CCR from diverse RSV strains, colored by linear epitope clustering in three regions. **(B)** Structure of RSV $G^{161-197}$, colored as in panel a, revealing the overlap of linear epitopes in three-dimensional space. **(C)** Table of 21 isolated human anti-G mAbs, their linear epitope sequences, and their RSV strain specificity.

MATERIALS AND METHODS

Study design

The overall objective of the study was to determine the molecular basis for antibody recognition of the RSV G glycoprotein. To enable this goal, we undertook experiments centered on protein chemistry, enzyme-linked immunosorbent assay (ELISA) binding studies, protein x-ray crystallography, and cellular chemotaxis assays. The number of independent experiments is outlined in figure legends and in Materials and Methods, where appropriate.

Production of bnmAbs 3D3 and 2D10, Fab 3D3, and scFv 2D10

Recombinant bnmAb 3D3 and bnmAb 2D10 were produced by transient transfection in Chinese hamster ovary (CHO) cells and purification by immobilized protein A, as described previously (22, 29). Fab 3D3 was generated by incubation of bnmAb 3D3 with immobilized papain, followed by removal of the Fc fragment with immobilized protein A. Fab 3D3 was then purified by Superdex 200 size exclusion chromatography in 10 mM tris-HCl (pH 8.0) and 150 mM NaCl. For recombinant scFv 2D10, a synthetic gene codon-optimized for Drosophila melanogaster—encoding the bnmAb 2D10 heavy-chain variable region, a $(GGGGS)_3GGG$ linker, and the bnmAb 2D10 light-chain variable region—was cloned into pMT-puro in-

frame with an N-terminal BiP signal sequence and a C-terminal thrombin cleavage site followed by a Twin-Strep purification tag. The resulting scFv 2D10 expression plasmid was used to obtain stably transfected Schneider 2 (S2) insect cells. Secreted scFv 2D10 was affinity-purified on a StrepTrap column, digested with thrombin protease to remove the purification tag, and then purified by Superdex 200 size exclusion chromatography in 10 mM tris-HCl (pH 8.0) and 150 mM NaCl.

Expression and purification of RSV G^{ecto}

A synthetic gene encoding RSV G (strain A2) amino acids 64 to 298 (UniProtKB entry P03423) was cloned into pCF in-frame with an N-terminal tissue plasminogen activator signal sequence and C-terminal tandem 6× histidine and Twin-Strep purification tags. Recombinant RSV $G^{ecto}$was produced by transient transfection in CHO cells, and secreted RSV G^{ecto} was affinity-purified on a StrepTrap column.

Expression and purification of RSV $G^{161-197}$

A synthetic gene codon-optimized for E. coli encoding RSV G (strain A2) amino acids 161 to 197 (UniProtKB entry P03423) with a C-terminal 6× histidine purification tag was cloned into pET52b. Recombinant RSV $G^{161-197}$ was expressed overnight in E. coli BL21(DE3) at 18°C. E. coli cells were lysed by ultrasonication in 20 mM tris-HCl (pH 8.0), 150 mM NaCl, and 25 mM imidazole (buffer A) containing 2 μM $MgCl_2$, benzonase, and protease inhibitors. RSV $G^{161-197}$ was purified from soluble lysates by HisTrap FF affinity chromatography and eluted with a gradient into

buffer B (buffer A containing 500 mM imidazole). The purification of soluble RSV $G^{161-197}$ in the absence of reducing agents appears to be sufficient for spontaneous formation of the cysteine noose disulfide bonds (1-4, 2-3 connectivity), as observed in the crystal structure of the Fab 3D3-RSV $G^{161-197}$ complex.

Enzyme-linked immunosorbent assay

Purified bnmAbs at a concentration of 5 μg/ml (150 μl total) were incubated overnight at room temperature in 96-well ELISA microtiter plates. Plates were then washed three times with PBS containing 0.05% Tween 20 (PBST). Wells were blocked by adding 150 μl of 5% bovine serum albumin (BSA) in PBS and incubating at room temperature for 1 hour followed by three PBST washes. Recombinant RSV G^{ecto} at 5 μg/ml or RSV $G^{161-197}$ at 20 μg/ml in 1% BSA in PBS was serially diluted 1:3 with 1% BSA in PBS. Wells were incubated with 150 μl of RSV G protein for 1 hour at room temperature, and the plates were washed three times with PBST. The plates were then incubated for 1 hour at room temperature with 150 μl of horseradish peroxidase–conjugated HisProbe (Thermo Fisher Scientific) diluted 1:5000 in 1% BSA in PBS. Plates were washed three times with PBST and developed by adding peroxidase substrate o-phenylenediamine dihydrochloride in 0.05 M phosphate-citrate buffer (pH 5.0) and 1.5% hydrogen peroxide for 10 min at room temperature. The reactions were stopped by incubation with 2N sulfuric acid for 10 min at room temperature, and the absorbance was measured at 490 nm. ELISA experiments were performed in biological triplicates.

Formation and structure determination of the Fab 3D3-RSV $G^{162-172}$ complex

A synthetic peptide encoding RSV G amino acids 162 to 172 (UniProtKB entry P03423) was mixed in 5-molar excess with purified Fab 3D3 at 17.5 mg/ml in 10 mM tris-HCl (pH 8.0) and 150 mM NaCl. Crystals were grown by hanging drop vapor diffusion at 4°C with a well solution of 23% PEG 3350 and 0.05 M zinc acetate. Crystals were transferred into a cryoprotectant solution of 26% PEG 3350, 0.05 M zinc acetate, and 25% ethylene glycol and flash-frozen in liquid nitrogen. Diffraction data were collected at cryogenic temperature at the Advanced Light Source (ALS) on beamline 8.3.1 using a wavelength of 1.11503 Å. Diffraction data from a single crystal were processed with iMosflm (36) and Aimless (table S1) (37). The Fab 3D3-RSV G162-172complex structure was solved by molecular replacement with a Fab homology model and the program PHASER (38), and the structure was refined and manually rebuilt using PHENIX (39) and Coot (40), respectively (table S1).

Formation and structure determination of the Fab 3D3-RSV $G^{161-197}$ complex

Purified RSV $G^{161-197}$ was mixed in 2-molar excess with purified Fab 3D3, dialyzed into 10 mM tris-HCl (pH 8.0) and 150 mM NaCl, and concentrated to 15 mg/ml. Crystals were grown by hanging drop vapor diffusion at 22°C with a well solution of 21% PEG 3350 and 0.2 M ammonium citrate (pH 7.0). Crystals were transferred into a cryoprotectant solution of 25% PEG 3350, 0.2 M ammonium citrate (pH 7.0), and 25% glycerol and flash-frozen in liquid nitrogen. Diffraction data were collected at cryogenic temperature at the ALS beamline 8.3.1 using a wavelength of 1.11582 Å.

Diffraction data were collected at cryogenic temperature at the ALS on beamline 8.3.1 using a wavelength of 1.11503 Å. Diffraction data from a single crystal were processed with iMosflm (36) and Aimless (37) (table S1). The Fab 3D3-RSV G161-197 complex structure was solved by molecular replacement with Fab 3D3 and the program PHASER (38), and the structure was refined and manually rebuilt using PHENIX (39) and Coot (40), respectively (table S1).

Formation and structure determination of the scFv 2D10-RSV $G^{169-198}$ complex

A synthetic peptide encoding RSV G amino acids 169 to 198 (UniProtKB entry P03423) was mixed in 2-molar excess with purified scFv in 60 mM tris-HCl (pH 8.0) and 230 mM NaCl and concentrated to 15.0 mg/ml. Crystals were grown by hanging drop vapor diffusion at 22°C with a well solution of 24% PEG 4000, 0.17 M ammonium sulfate, 0.085 M sodium citrate (pH 5.6), and 15% glycerol. Crystals were transferred into a cryoprotectant solution of 28% PEG 4000, 0.17 M ammonium sulfate, 0.085 M sodium citrate (pH 5.6), 15% glycerol, and 25% glycerol and flash-frozen in liquid nitrogen. Diffraction data were collected at cryogenic temperature at the Advanced Photon Source on beamline 23-ID-D using a wavelength of 1.033 Å. Diffraction data from a single crystal were processed with HKL2000 (table S1) (41). The scFv 2D10-RSV G169-198complex structure was solved by molecular replacement with a scFv homology model and the program PHASER (38), and the structure was refined and manually rebuilt using PHENIX (39) and Coot (40), respectively (table S1).

Chemotaxis assay

The in vitro chemotaxis assay was performed using a Transwell insert plate with an 8-μm pore size, following previously published methods (9, 23). Approximately 2 million log-phase THP-1 cells (a human leukemia monocytic cell line) washed twice and suspended in serum-free RPMI 1640 media were added to the upper chamber of the insert plate. Negative controls were serum-free media alone or serum-free media containing 25 nM bnmAb 3D3 or bnmAb 2D10 was added to the lower chamber. As a positive control, media containing 10% fetal bovine serum (FBS) was added to the lower chamber. RSV G^{ecto} or RSV $G^{161-197}$ samples were added to the lower chamber at a final concentration of 5 nM in serum-free media. For samples with RSV $G^{161-197}$and bnmAbs, RSV $G^{161-197}$ was preincubated with 5-molar excess bnmAb for 20 min at room temperature and then added to serum-free media in the lower chamber for a final concentration of 5 nM RSV $G^{161-197}$ and 25 nM bnmAb. For samples with anti-CX3CR1 antibody, 2 μl anti-CX3CR1 rabbit polyclonal antibody (1 mg/ml) was incubated with THP-1 cells for 30 min in the upper chamber before being placed into the well. The anti-CX3CR1 rabbit polyclonal antibody (cat no. PA5-19910; Thermo Fisher Scientific) was generated by immunization of rabbits with a peptide corresponding to amino acids 2 to 21 of human CX3CR1 (UniProt ID P49238). The assembled plates were incubated in a CO_2 incubator at 37°C for 5 hours. Cells migrated to the lower chamber were counted, and the chemotactic indices were determined by comparing the fold increase in cell migration toward the

chemoattractant to cell migration toward serum-free media alone. Experiments were performed in at least four biological replicates.

For chemotaxis assays with CX3CL1 (fractalkine), THP-1 cells were washed and suspended in serum-free RPMI 1640 media containing BSA (1 mg/ml). Recombinant full-length human CX3CL1 (cat no. 365-FR; R&D Systems) was added to the lower chamber at a final concentration of 10 nM. For samples with bnmAbs, CX3CL1 was preincubated with 2.5 M excess bnmAb for 20 min at room temperature and then added to the lower chamber for a final concentration of 10 nM CX3CL1 and 25 nM bnmAb. For samples with anti-CX3CR1 antibody, 2 μl anti-CX3CR1 rabbit polyclonal antibody (1 mg/ml) was incubated with THP-1 cells for 30 min in the upper chamber before being placed into the well. Experiments were performed in four biological replicates.

ACKNOWLEDGMENTS

We thank S. Tripathi for assistance in crystallographic data collection and structure determination, D. Alexander for assistance in RSV Gecto expression, P. Berman for use of laboratory equipment, and R. Tripp for advice. Funding: R.M.D. is supported by the National Institute of Allergy and Infectious Diseases (NIAID) grant R21AI130605. L.M.K. acknowledges partial support from NIAID grant 5R44AI122360-02. This research used resources of the ALS, which is a U.S. Department of Energy (DOE) Office of Science User Facility under contract no. DE-AC02-05CH11231. Data collection at the ALS Beamline 8.3.1 is supported by the University of California Office of the President, Multicampus Research Programs and Initiatives Grant MR-15-328599 and Program for Breakthrough Biomedical Research, which is partially funded by the Sandler Foundation. This research also used resources of the Advanced Photon Source, a DOE Office of Science User Facility operated for the DOE Office of Science by Argonne National Laboratory under contract no. DE-AC02-06CH11357. Author contributions: S.O.F. produced bnmAb 2D10 and RSV Gecto, produced antibody/G complexes, solved crystal structures, and performed ELISA experiments and chemotaxis assays. N.L.G. and J.T.W. produced RSV G161-197 and scFv 2D10. S.O.F. and R.M.D. carried out statistical analyses. L.M.K. contributed purified bnmAb 3D3. R.M.D. conceived the experiments and wrote the manuscript with S.O.F. and L.M.K. Competing interests: L.M.K. is an employee of and holds an equity interest in Trellis Bioscience,

which is preparing mAb 3D3 for clinical evaluation, and is an inventor on US patents relating to mAb 3D3: Nos. 7,736,648; 8,273,354; 9,321,830. L.M.K., R.M.D., and S.O.F. are inventors on US patent filing No. 62/588,022. All other authors declare that they have no competing interests.

Data and materials availability: The atomic coordinates and structure factors have been deposited in the Protein Data Bank, www.pdb.org, under accession codes 5WN9, 5WNA, and 5WNB.

Table S1. Crystallographic data collection and refinement statistics

	3D3-RSV G$^{162-172}$	**3D3-RSV G$^{161-197}$**	**2D10-RSV G$^{169-198}$**
PDB code	5WNB	5WNA	5WN9
Data collection[a,b]			
Space group	P 21 21 21	P 1 21 1	P 21 21 21
Cell dimensions			
a, *b*, *c* (Å)	68.76, 105.43, 121.82	64.62, 135.01, 73.78	44.84, 56.39, 126.15
α, β, γ (°)	90.00, 90.00, 90.00	90.00, 107.45, 90.00	90.00, 90.00, 90.00
Resolution (Å)	48.38 - 2.40 (2.48 – 2.40)	48.72 - 2.40 (2.48 - 2.40)	50.00 - 1.55 (1.58 – 1.55)
R_{sym} or R_{merge}	0.122 (0.838)	0.107 (0.763)	0.058 (0.930)
I / σI	13.4 (3.1)	12.3 (2.2)	44.0 (1.4)
Completeness (%)	99.9 (99.8)	99.5 (99.0)	99.9 (99.4)
Redundancy	9.2 (8.3)	6.3 (5.6)	9.6 (6.2)
$CC_{1/2}$	0.997 (0.808)	0.996 (0.670)	0.998 (0.751)
Refinement			
Resolution (Å)	48.38 - 2.40	48.72 - 2.40	50.00 - 1.55
No. reflections	35,325	46,869	47,114
R_{work} / R_{free}[c]	0.218 / 0.280	0.192 / 0.246	0.169 / 0.185
No. atoms			
Protein	6,586	7,124	3,810
Ligand/ion	22	None	None
Water	90	135	111
B-factors			
Protein	50.29	42.02	34.04
Ligand/ion	63.66	None	None
Water	35.5	38.59	37.92
R.m.s. deviations			
Bond lengths (Å)	0.005	0.006	0.008
Bond angles (°)	0.864	0.935	0.968

[a] For each structure, data from one crystal was used.
[b] Values in parentheses are for highest-resolution shell.
[c] R_{free} was calculated using 5% of data excluded from refinement.

REFERENCES:

1. W. P. Glezen, L. H. Taber, A. L. Frank, J. A. Kasel, Risk of primary infection and reinfection with respiratory syncytial virus. Am J Dis Child 140, 543-546 (1986).
2. S. Jain et al., Community-acquired pneumonia requiring hospitalization among U.S. children. The New England journal of medicine 372, 835-845 (2015).
3. T. Shi et al., Global, regional, and national disease burden estimates of acute lower respiratory infections due to respiratory syncytial virus in young children in 2015: a systematic review and modelling study. Lancet 390, 946-958 (2017).
4. C. B. Hall et al., The burden of respiratory syncytial virus infection in young children. The New England journal of medicine 360, 588-598 (2009).
5. R. Lozano et al., Global and regional mortality from 235 causes of death for 20 age groups in 1990 and 2010: a systematic analysis for the Global Burden of Disease Study 2010. Lancet 380, 2095-2128 (2012).
6. Palivizumab, a Humanized Respiratory Syncytial Virus Monoclonal Antibody, Reduces Hospitalization From Respiratory Syncytial Virus Infection in High-risk Infants. Pediatrics 102, 531-537 (1998).

7. C. Capella et al., Prefusion F, postfusion F, G antibodies and disease severity in infants and young children with acute respiratory syncytial virus infection. The Journal of infectious diseases, (2017).
8. J. S. McLellan et al., Structure-based design of a fusion glycoprotein vaccine for respiratory syncytial virus. Science 342, 592-598 (2013).
9. R. A. Tripp, U. F. Power, P. J. M. Openshaw, L. M. Kauvar, Respiratory Syncytial Virus (RSV): Targeting the G Protein Provides a New Approach for an Old Problem. Journal of virology 92:e01302-17, (2017).
10. S. M. Johnson et al., Respiratory Syncytial Virus Uses CX3CR1 as a Receptor on Primary Human Airway Epithelial Cultures. PLoS pathogens 11, e1005318 (2015).
11. T. Chirkova et al., CX3CR1 is an important surface molecule for respiratory syncytial virus infection in human airway epithelial cells. The Journal of general virology 96, 2543-2556 (2015).
12. K. I. Jeong et al., CX3CR1 Is Expressed in Differentiated Human Ciliated Airway Cells and Co-Localizes with Respiratory Syncytial Virus on Cilia in a G Protein-Dependent Manner. PloS one 10, e0130517 (2015).
13. R. A. Tripp et al., CX3C chemokine mimicry by respiratory syncytial virus G glycoprotein. Nature immunology 2, 732-738 (2001).
14. D. A. Hendricks, K. Baradaran, K. McIntosh, J. L. Patterson, Appearance of a soluble form of the G protein of respiratory syncytial virus in fluids of infected cells. The Journal of general virology 68 (Pt 6), 1705-1714 (1987).

15. D. A. Hendricks, K. McIntosh, J. L. Patterson, Further characterization of the soluble form of the G glycoprotein of respiratory syncytial virus. Journal of virology 62, 2228-2233 (1988).

16. R. Arnold, B. Konig, H. Werchau, W. Konig, Respiratory syncytial virus deficient in soluble G protein induced an increased proinflammatory response in human lung epithelial cells. Virology 330, 384-397 (2004).

17. J. Harcourt et al., Respiratory syncytial virus G protein and G protein CX3C motif adversely affect CX3CR1+ T cell responses. J Immunol 176, 1600-1608 (2006).

18. L. M. Haynes, L. P. Jones, A. Barskey, L. J. Anderson, R. A. Tripp, Enhanced disease and pulmonary eosinophilia associated with formalin-inactivated respiratory syncytial virus vaccination are linked to G glycoprotein CX3C-CX3CR1 interaction and expression of substance P. Journal of virology 77, 9831-9844 (2003).

19. M. N. Teng, S. S. Whitehead, P. L. Collins, Contribution of the respiratory syncytial virus G glycoprotein and its secreted and membrane-bound forms to virus replication in vitro and in vivo. Virology 289, 283-296 (2001).

20. S. Boyoglu-Barnum et al., Mutating the CX3C motif in the G protein should make a live respiratory syncytial virus vaccine safer and more effective. Journal of virology, (2017).

21. L. J. Anderson, J. C. Hierholzer, Y. O. Stone, C. Tsou, B. F. Fernie, Identification of epitopes on respiratory syncytial virus proteins by

competitive binding immunoassay. Journal of clinical microbiology 23, 475-480 (1986).

22. E. J. Collarini et al., Potent high-affinity antibodies for treatment and prophylaxis of respiratory syncytial virus derived from B cells of infected patients. J Immunol 183, 6338-6345 (2009).

23. H. J. Lee, J. Y. Lee, M. H. Park, J. Y. Kim, J. Chang, Monoclonal Antibody against G Glycoprotein Increases Respiratory Syncytial Virus Clearance In Vivo and Prevents Vaccine-Enhanced Diseases. PloS one 12, e0169139 (2017).

24. B. Cortjens et al., Broadly Reactive Anti-Respiratory Syncytial Virus G Antibodies from Exposed Individuals Effectively Inhibit Infection of Primary Airway Epithelial Cells. Journal of virology 91, (2017).

25. S. Boyoglu-Barnum et al., An anti-G protein monoclonal antibody treats RSV disease more effectively than an anti-F monoclonal antibody in BALB/c mice. Virology 483, 117-125 (2015).

26. H. Caidi, J. L. Harcourt, R. A. Tripp, L. J. Anderson, L. M. Haynes, Combination therapy using monoclonal antibodies against respiratory syncytial virus (RSV) G glycoprotein protects from RSV disease in BALB/c mice. PloS one 7, e51485 (2012).

27. L. M. Haynes et al., Therapeutic monoclonal antibody treatment targeting respiratory syncytial virus (RSV) G protein mediates viral clearance and

reduces the pathogenesis of RSV infection in BALB/c mice. The Journal of infectious diseases 200, 439-447 (2009).

28. G. U. Radu et al., Prophylactic treatment with a G glycoprotein monoclonal antibody reduces pulmonary inflammation in respiratory syncytial virus (RSV)-challenged naive and formalin-inactivated RSV-immunized BALB/c mice. Journal of virology 84, 9632-9636 (2010).

29. L. M. Kauvar, E. J. A Collarini, B. A Keyt, O. A Foord, Anti-RSV G protein antibodies. Patent number US 8273354, (2010).

30. M. Sugawara et al., Structure-antigenicity relationship studies of the central conserved region of human respiratory syncytial virus protein G. The journal of peptide research : official journal of the American Peptide Society 60, 271-282 (2002).

31. J. F. Doreleijers et al., Solution structure of the immunodominant region of protein G of bovine respiratory syncytial virus. Biochemistry 35, 14684-14688 (1996).

32. B. Shields, J. Mills, R. Ghildyal, P. Gooley, J. Meanger, Multiple heparin binding domains of respiratory syncytial virus G mediate binding to mammalian cells. Archives of virology 148, 1987-2003 (2003).

33. I. Kufareva, C. L. Salanga, T. M. Handel, Chemokine and chemokine receptor structure and interactions: implications for therapeutic strategies. Immunology and cell biology 93, 372-383 (2015).

34. S. S. Lieberman-Blum, H. B. Fung, J. C. Bandres, Maraviroc: a CCR5-receptor antagonist for the treatment of HIV-1 infection. Clinical therapeutics 30, 1228-1250 (2008).

35. S. Fuentes, E. M. Coyle, J. Beeler, H. Golding, S. Khurana, Antigenic Fingerprinting following Primary RSV Infection in Young Children Identifies Novel Antigenic Sites and Reveals Unlinked Evolution of Human Antibody Repertoires to Fusion and Attachment Glycoproteins. PLoS pathogens 12, e1005554 (2016).

36. T. G. Battye, L. Kontogiannis, O. Johnson, H. R. Powell, A. G. Leslie, iMOSFLM: a new graphical interface for diffraction-image processing with MOSFLM. Acta Crystallogr D Biol Crystallogr 67, 271-281 (2011).

37. P. R. Evans, G. N. Murshudov, How good are my data and what is the resolution? Acta Crystallogr D Biol Crystallogr 69, 1204-1214 (2013).

38. A. J. McCoy et al., Phaser crystallographic software. Journal of applied crystallography 40, 658-674 (2007).

39. P. D. Adams et al., PHENIX: a comprehensive Python-based system for macromolecular structure solution. Acta Crystallogr D Biol Crystallogr 66, 213-221 (2010).

40. P. Emsley, K. Cowtan, Coot: model-building tools for molecular graphics. Acta Crystallogr D Biol Crystallogr 60, 2126-2132 (2004).

41. Z. Otwinowski, W. Minor, Charles W. Carter, Jr., in Methods Enzymol. (Academic Press, 1997), vol. 276, pp. 307-326.

Chapter II

Conformational flexibility in respiratory syncytial virus G neutralizing epitopes

ABSTRACT

Respiratory syncytial virus (RSV) is a top cause of severe lower respiratory tract disease and mortality in infants and the elderly. Currently, no vaccine or effective antiviral treatment exists for RSV. The RSV G glycoprotein mediates viral attachment to cells and contributes to pathogenesis by modulating host immunity through interactions with the human chemokine receptor CX3CR1. Antibodies targeting the RSV G central conserved domain are protective in both prophylactic and post-infection animal models. Here, we describe the crystal structure of the broadly-neutralizing monoclonal antibody 3G12 bound to the RSV G central conserved domain. Antibody 3G12 binds to a conformational epitope comprised of highly conserved residues, explaining its broad neutralization activity. Surprisingly, RSV G complexed with 3G12 adopts a distinct conformation not observed in previously described RSV G–antibody structures. Comparison to other structures reveals that the RSV G central conserved domain is flexible and capable of adopting multiple conformations in the regions flanking the cysteine noose region. We also show that antibody 3G12 blocks RSV G-mediated cell chemotaxis, providing a mechanistic basis for its ability to protect against RSV infection and disease in vivo. Our studies

support the development of RSV G as a vaccine antigen. Moreover, our studies provide new insights for rational vaccine design, indicating the importance of preserving the global structural integrity of antigens, yet at the same time preserving local conformational flexibility at antigenic sites which may facilitate a more diverse antibody response and provide broader protection against infection and disease.

IMPORTANCE

Respiratory syncytial virus (RSV) causes severe respiratory infections in infants, young children, and the elderly, and currently no licensed vaccine exists. In this study, we describe the crystal structure of the RSV surface glycoprotein G in complex with a broadly-neutralizing monoclonal antibody. The antibody binds to RSV G at a highly conserved region, which is stabilized by two disulfide bonds, but captures RSV G in a conformation not previously observed, revealing that this region is both structured and flexible. Importantly, our findings provide insight for the design of vaccines that elicit diverse antibodies that provide broad protection from infection and disease.

INTRODUCTION

Respiratory syncytial virus (RSV) is a globally prevalent respiratory virus which affects the lungs and airways. Infants and young children are at the highest risk of severe outcome from RSV infection, with 33.1 million episodes of lower respiratory tract infection and approximately 3.2 million hospital visits and 118,200 deaths per year worldwide in children under age 5 due to RSV (1). RSV is also a major cause of illness in adults older than 65 years and immunocompromised individuals, with an estimated 14,000 deaths per year in the United States (2). Hospitalization due to RSV is a major economic burden, especially in preterm infants and older adults (3).

Currently, no licensed vaccine exists for the prevention of RSV infection, making RSV one of the highest burden diseases with no readily available preventative measure. The only FDA-approved therapy for RSV is passive prophylaxis with palivizumab (Synagis), a monoclonal antibody which reduces disease severity and hospitalization (4). Palivizumab's approved use is limited to high-risk premature birth infants; due to the high cost, approximately $10,000 for a full course of therapy (5), it is not widely used in low-income countries. The need for widely available vaccines and therapies for RSV is evidenced from the 19 vaccine candidates and therapeutic monoclonal antibodies in clinical trials (6).

RSV is a negative-sense single stranded RNA virus with two major glycoproteins on the virion surface: the attachment glycoprotein (G) and the fusion glycoprotein (F) (7). RSV G is responsible for cellular attachment to host cells and

RSV F causes the viral membrane to fuse with the target host cell membrane. While both RSV F and G are immunogenic and are targeted by neutralizing antibodies, the majority of neutralizing antibodies in human sera target RSV F (8, 9). As such, most RSV vaccine candidates and therapeutic antibodies currently in development focus on RSV F. However, RSV that does not express the G protein is highly attenuated *in vivo* (10), and monoclonal antibodies that target RSV G are protective *in vivo* (11-21). In humans, anti-G antibodies are associated with lower clinical disease severity scores, despite an abundance in sera more than 30 times lower than anti-F antibodies (8). Thus, the RSV G protein is increasingly recognized as an important target for RSV vaccine and therapeutic antibody development (22).

RSV G is a type II membrane protein containing two mucin-like regions coated with 30-40 O-linked glycans and 3-5 N-linked glycans (Fig. 1A) (7, 23, 24). There are two forms of RSV G produced during infection. Membrane-bound RSV G is responsible for virus attachment to airway epithelial cells via the human chemokine receptor CX3CR1 (25-28). A secreted form of RSV G, derived from a second translation initiation site at Met48 and released from the membrane by proteolysis, is expressed early in the infection (first ~6 hours, prior to the release of virions at ~12 hours) (Fig. 1A) (29). Secreted RSV G modulates signaling and trafficking of $CX3CR1^{+}$ immune cells, contributing to airway congestion and pathogenesis (26, 27, 30-33). Between the two mucin-like regions of RSV G is a central conserved domain (CCD) of ~40 highly conserved amino acids, including four invariant cysteines forming a cysteine noose motif with two disulfide bonds (1-4, 2-3

connectivity) (Fig. 1A) (34-36). While the C-terminus of the RSV G CCD possesses a heparin binding domain (Fig. 1A) (37, 38), initial RSV infection is thought to be mediated primarily by interaction between the RSV G CCD and CX3CR1 on ciliated lung cells (25-28), which do not have measurable heparan sulfate proteoglycans on their surfaces.

Broadly neutralizing monoclonal antibodies (bnmAbs) that target RSV G are able to neutralize RSV infectivity in cell culture, including in HAE cells, and significantly reduce RSV viral loads and disease in both prophylactic and post-infection animal models (12, 14-16, 21, 25, 28, 39, 40). In addition to reducing viral loads, treatment with anti-RSV G mAbs reduces BAL cell influx including RSV G protein-induced leukocyte migration and eosinophilic inflammatory response, resulting in decreased airway congestion (15, 33, 41). Anti-G mAbs have also been shown to reduce mucus production and to restore beneficial antiviral IFN-α (18, 41-43). Most of the anti-G bnmAbs that have been studied to date bind with high affinity to RSV G (K_D (dissociation constant) = 1.1 pm - 3.3 nM) and bind to linear epitopes within the RSV G CCD, as determined by linear epitope mapping techniques (17, 21, 39, 44). Recently, two studies elucidated four high-resolution crystal structures of antibody-RSV G CCD complexes (16, 45). Unexpectedly, all four antibodies were found to bind to conformational epitopes, revealing additional interactions beyond their linear epitopes and illuminating a previously unappreciated role of the disulfide-stabilized cysteine noose in forming conformational epitopes and contributing to high-affinity antibody binding.

Here, we investigated the bnmAb 3G12, which reduces viral loads, airway hyper-responsiveness, and inflammation in both prophylactic and post-infection mouse models of RSV infection despite binding with ~100-fold weaker affinity than the previously studied bnmAbs (12, 21). Linear epitope mapping experiments have shown that bnmAb 3G12 binds to RSV G CCD residues 167-176, which is shifted downstream compared to other anti-G bnmAbs in the panel that bind primarily RSV G residues 162-169 (12, 21). We hypothesized that structural studies into the 3G12 antigenic site might reveal additional information about the mechanisms of high-affinity antibody binding and broad neutralization against RSV A and B strains. We present here the structure of antibody 3G12 bound to the RSV G CCD, which reveals a novel conformational epitope comprised of highly conserved residues. The structure reveals that the RSV G CCD is flexible and adopts several distinct conformations. We also show that antibody 3G12 blocks RSV G chemotactic activity, providing a mechanistic basis for its ability to protect against RSV infection and disease *in vivo*. Overall, these studies have broad implications for vaccine design, highlighting the importance of maintaining flexibility in vaccine antigen epitopes so as to elicit diverse antibody responses.

RESULTS

Fab 3G12-RSV $G^{157-197}$ complex structure

We investigated bnmAb 3G12, a native human antibody that binds RSV G with high affinity, K_D = 579 pM. Antibody 3G12 shows broadly neutralizing activity

across diverse lab and clinical RSV strains (21). To understand the molecular basis for the broad reactivity of bnmAb 3G12 and to determine if it binds to a larger conformational epitope beyond that predicted by linear epitope mapping, we used X-ray crystallographic studies to determine the structure of bnmAb 3G12 bound to the RSV G CCD (Fig. 1A). Purified antigen-binding fragment (Fab) 3G12 was mixed with recombinant RSV $G^{157-197}$, which formed a stable complex in solution. We crystallized the Fab 3G12-RSV $G^{157-197}$ complex and determined its crystal structure to 2.9 Å resolution (Fig. 1B, Fig 1C and Table 2).

The Fab 3G12-RSV $G^{157-197}$ complex structure reveals a 924 $Å^2$ epitope on the RSV G CCD, with 3G12 heavy chain burying 697 $Å^2$ and the light chain burying 227 $Å^2$ of the epitope (Fig. 1B). Similar to RSV G-antibody structures determined previously (16, 45), antibody 3G12 binds to a *conformational epitope* comprised of RSV G residues 160-179, 182 and 189, revealing additional interactions beyond the linear epitope residues 167-176 (Fig. 1). The linear epitope residues are invariant or highly conserved (Fig. 1A), explaining the broad reactivity of bnmAb 3G12 for diverse RSV strains. The 3G12 heavy chain complementarity-determining regions (HCDRs) account for the majority of the interactions and buried surface with the RSV G CCD, with the HCDR2 burying the largest portion with 315 $Å^2$ and HCDR3 accounting for 284 $Å^2$ (Fig. 1C). On the light chain complementarity-determining regions (LCDRs), LCDR3 buries 169.5 $Å^2$ on the N-terminal end of the RSV G CCD, while LCDR1 and the Fab 3G12 N-terminal residues form additional minor interactions (Fig. 1C). The 3G12 heavy chain CDR2 stabilizes residues 167-170 of

RSV G by several hydrogen bonds and van der Waals interactions. In addition, residues from all three of the HCDRs from bnmAb 3G12 stabilize hydrophobic interactions with RSV G residues F163, F165, F168, F170, P172, and I175, forming a hydrophobic core-like region within the antibody 3G12-RSV G complex. Interestingly, the helix on the C-terminal end of the cysteine noose, which encompasses the CX3C motif (residues 180-186) has almost no interactions with antibody 3G12, unlike other antibody-RSV G CCD structures, where this helix has a role in antibody binding (Fig.1C and Fig. 2).

RSV G CCD epitopes and conformational flexibility

To better understand the conformational flexibility in the RSV G CCD, all known structures of the CCD bound by antibodies were compared (Fig. 2). The structures were aligned at the cysteine noose region (~ residues 170-187), which has an RMSD of <0.6 Å across all structures. The region N-terminal to the cysteine noose (~ residues 160-169) adopts a different conformation in each structure (RMSD of 3-5 Å) and varies in secondary structural elements (i.e. forms a helix when bound to antibody 3D3 and forms a strand when bound to antibody CB002.5)(Fig. 2). RSV G residue N169 appears to be flexible across all of the structures and may be one of the last semi-ordered residues in the N-terminal region of the CCD. Similarly, the C-terminal region after K187 may be flexible and capable of adopting multiple conformations (Fig. 2). These C-terminal, non-interacting RSV G CCD residues are present in most of the complexes but do not have visible electron density, suggesting

that they are dynamic and flexible. Overall, the RSV G CCD cysteine noose is structurally conserved and forms an important structural element for antibody binding, however the N- and C-terminal regions of the CCD are flexible and adopt different conformations when captured by diverse antibodies.

Biological relevance of the 3G12 epitope

To understand the mechanism by which bnmAb 3G12 protects against RSV infection and disease *in vivo*, we performed an *in vitro* chemotaxis assay in human monocyte THP-1 cells. Previously, we showed that recombinant RSV G ectodomain (RSV G^{ecto}) and RSV G CCD induce THP-1 cell chemotaxis, and anti-CX3CR1 antibodies inhibited chemotaxis (45). Here, we confirmed that RSV G^{ecto} stimulates chemotaxis ~5 times over background levels (Fig. 3). Preincubation of RSV G^{ecto} with bnmAb 3G12 mAb suppresses the chemotactic activity to levels similar to negative control (Fig. 3). Control experiments show that bnmAb 3G12 alone has no effect on chemotaxis. These experiments demonstrate that bnmAb 3G12 blocks the chemotactic activity of RSV G, consistent with the activities of other bnmAbs targeting the CCD.

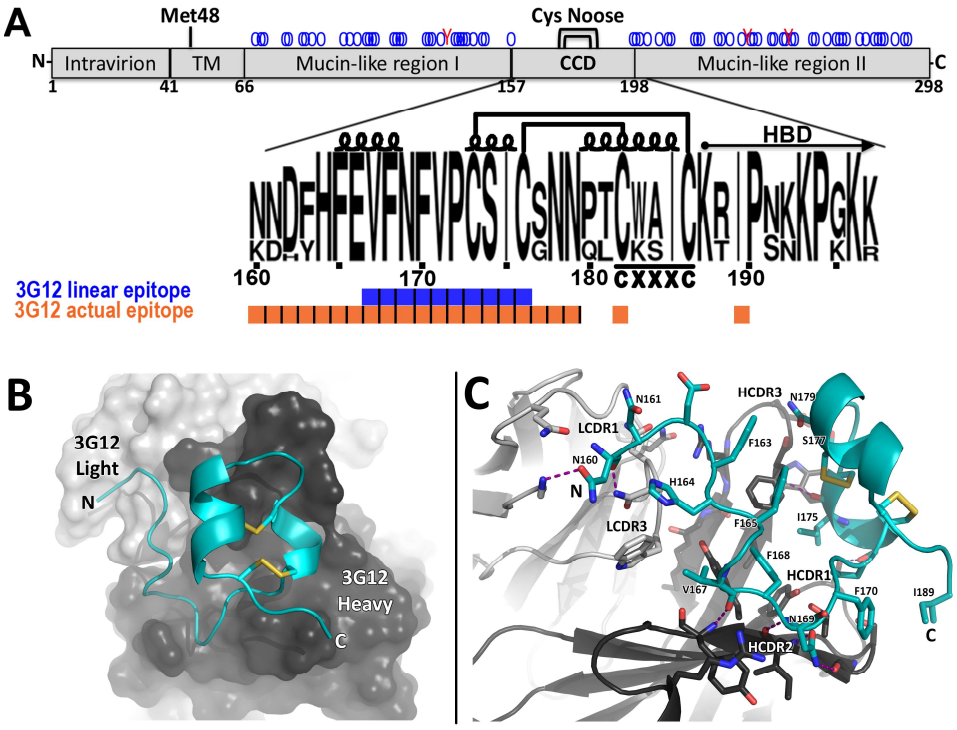

Fig. 2.1. Fab 3G12+RSV $G^{157-197}$ complex structure

Crystal structure of the Fab 3G12-RSV $G^{157-197}$ complex. (A) Schematic of the RSV G glycoprotein from RSV strain A2, including the transmembrane region (TM), CCD, and the cysteine noose (Cys noose). Met48 is the alternate initiation site for the production of soluble RSV G. Predicted N- and O-linked glycans are shown by red "Y" and blue "O," respectively. Below is a sequence logo of residues 160-197 of the RSV G CCD, revealing the sequence conservation across strains RSV A, RSV B, RSV L, and RSV 1-8. (B) Overall view of antibody 3G12 heavy chain (dark grey) and light chain (light grey) bound to RSV $G^{157-197}$ (cyan, with disulfides in yellow). (C) Zoom-in view of interactions between antibody 3G12 with RSV G CCD. Hydrogen bonds are shown as dashes. Heavy-chain CDRs (HCDR1-3) and light-chain CDRs (LCDR1 and 3) are labeled.

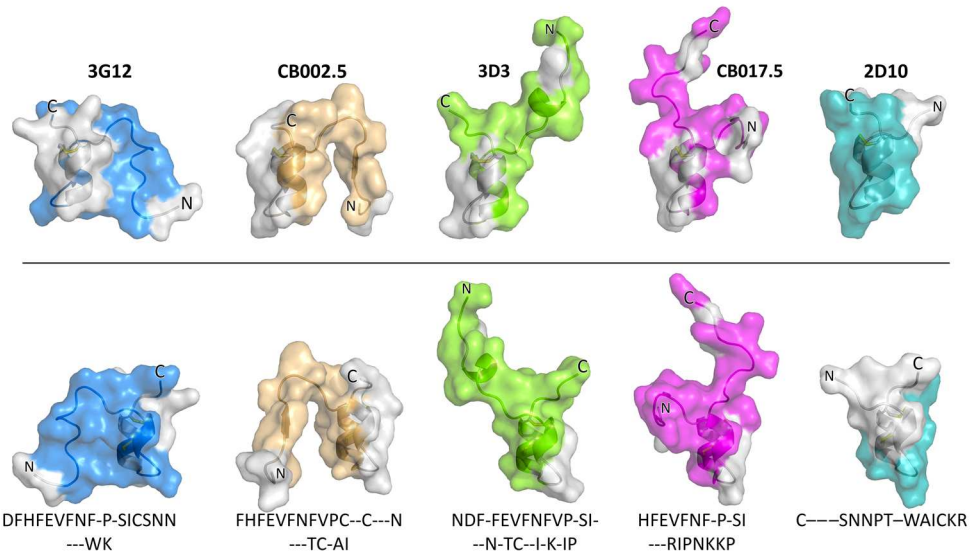

Fig. 2.2. All RSV G structures bound by antibodies and epitopes.

Comparison of known RSV G CCD epitopes and structures. Top, epitopes on RSV G are colored as follows: 3G12 (blue), CB002.5 (gold), 3D3 (green), CB017.5 (magenta), 2D10 (cyan). Bottom, 180 degree rotation around y-axis. Residues interacting with antibodies are written below each structure.

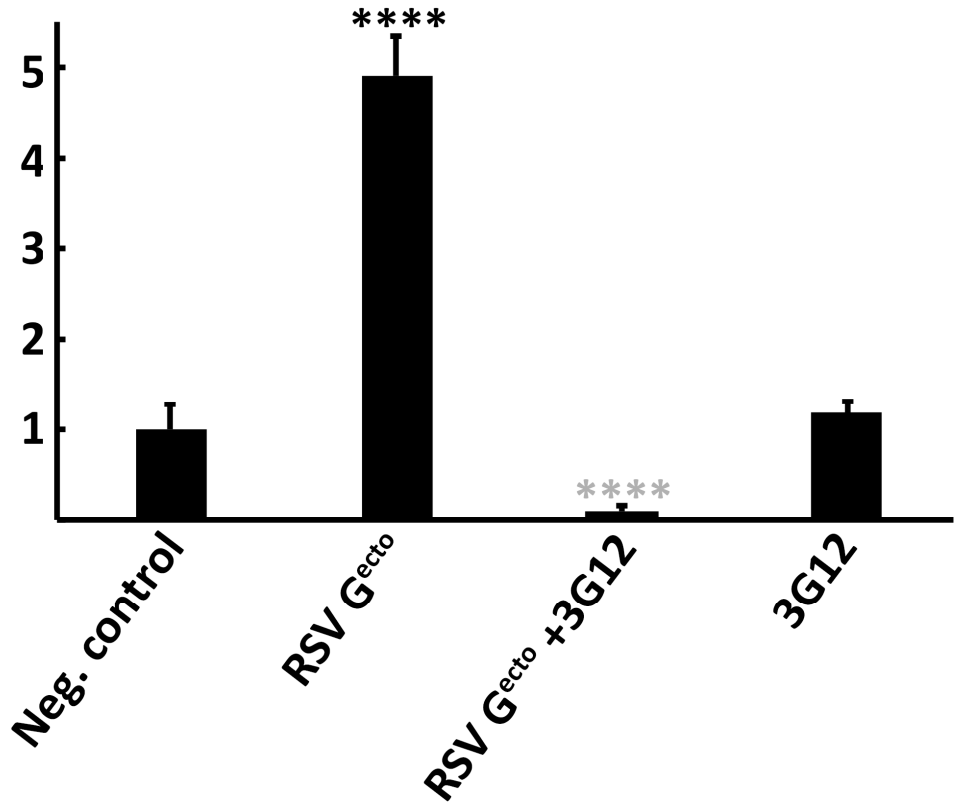

Fig. 2.3 bnmAbs 3G12 blocks RSV Gecto–induced chemotaxis.

bnmAb 3G12 blocks RSV G^{ecto}–induced chemotaxis. Serum-free media was used as negative control for the chemotaxis assay. Chemotactic indices were determined by comparing the fold increase in cell migration toward the chemoattractant compared to cell migration toward serum-free media alone. Studies with bnmAb 3G12 were used to examine inhibition of RSV G^{ecto}–induced chemotaxis. A student's t-test was performed. Black asterisks denote significance compared to negative control and gray asterisks denote significance compared to RSV G^{ecto} (****$P < 0.0001$). Chemotaxis experiments were performed in three biological replicates. Error bars indicate SEM.

DISCUSSION

Here, we describe the crystal structure of the human bnmAb 3G12 bound to the RSV G CCD, and we show that bnmAb 3G12 blocks RSV G-mediated cell chemotaxis. The antibody binds to a conformational epitope comprised of highly conserved residues, explaining its broad reactivity to diverse strains of RSV. The antibody interacts mainly with the RSV G CCD's N-terminal region, which adopts a distinct conformation that differs from all other known CCD structures, suggesting that the RSV G CCD is flexible outside of its rigid disulfide bonded cysteine noose region. Residue N169 likely represents a 'hinge' residue, where the N-terminal region of the CCD preceding N169 appears to be flexible and capable of adopting multiple conformations and even secondary structures. Likewise, residues after K187 in the C-terminal region of the CCD also appear to be flexible and capable of adopting multiple conformations.

The observation of different conformations of RSV G CCD raises several important questions. Does RSV G move freely and randomly, and do our structures reveal momentary snapshots captured by antibody binding? Alternatively, do individual RSV G molecules adopt one of several distinct conformations on the RSV surface? What conformation does RSV G adopt when interacting with the human CX3CR1 receptor? We note that none of the conformations have any substantial tertiary structure stabilizing interactions within the CCD or clearly defined secondary structure. Therefore it is unlikely that RSV G assumes distinct conformations without additional external stabilizing interactions. One form of stabilization may come from

the oligomerization state of RSV G. It has been previously suggested that RSV G exists as a trimer or tetramer (46, 47). The extensive glycosylation of RSV G in the mucin-like regions flanking the CCD may also restrict RSV G flexibility. It is also possible that RSV G interacts with RSV F on the virus surface, creating a quaternary structure which may provide RSV G with the defined structures like those captured by the antibodies discussed in this paper. If any of these possibilities are the case, then this has important implications for vaccine design since immunizing with RSV G or RSV G CCD alone may not elicit a native-like anti-G antibody response (48).

Our study also has important implications for vaccine antigen design in a broader sense. Recently, there has been a general trend in vaccine development for antigen stabilization. In HIV gp120, certain stabilizing mutations (SOSIP.v5.2 S306L/R308L) improve the productive neutralizing immune response in rabbits while reducing the immunogenicity of non-neutralizing epitopes (49). For influenza HA, several stabilized immunogens have been designed that elicit universal (cross-subtype) antibody responses and protection (50-54). In other cases, stabilization strategies have been key to locking viral membrane fusion protein antigens in the prefusion form, as was accomplished for Middle East respiratory syndrome coronavirus, human parainfluenza viruses, and RSV (55-57). In all cases, the pre-fusion stabilized antigens elicited higher levels of neutralizing antibodies compared to the post-fusion antigens. However, despite the many reports that stabilizing strategies can provide an effective and improved immune response, we caution that antigen stabilization could limit the *diversity* of antibody responses. Our study and others (58,

59) illuminate how antigens can have flexible, dynamic epitopes, and that diverse antibodies can target these epitopes in distinct ways. Thus, we recommend balancing the needs to stabilize antigens with the benefits of preserving the native flexibility of epitopes, which may help elicit a broader and more diverse immune response that may in turn offer better protection against virus escape. Incorporating antibody repertoire sequencing technologies during vaccine development could provide opportunities to evaluate antibody diversity that is elicited by stabilized antigens.

MATERIALS AND METHODS

Production of bnmAb 3G12 and Fab 3G12. Recombinant bnmAb 3G12 was produced by transient-transfection in CHO cells and purification by immobilized protein A, as described previously (21, 44). Fab 3G12 was generated by incubation of bnmAb 3G12 with immobilized papain, followed by removal of the Fc fragment with immobilized protein A. Fab 3G12 was then purified by Superdex 200 size-exclusion chromatography in 10 mM Tris-HCl pH 8.0 and 150 mM NaCl.

Expression and purification of RSV $G^{157-197}$. A synthetic gene codon-optimized for E. coli encoding RSV G (strain A2) amino acids 157 to 197 (UniProtKB entry P03423) with a C-terminal 6× histidine purification tag was cloned into pET52b. Recombinant RSV $G^{157-197}$ was expressed overnight in E. coli BL21(DE3) at 18°C. E. coli cells were lysed by ultrasonication in 20 mM Tris-HCl (pH 8.0), 150 mM NaCl, and 25 mM imidazole (buffer A) containing 2 μM MgCl2, benzonase, and protease

inhibitors. RSV $G^{157-197}$ was purified from soluble lysates by HisTrap FF affinity chromatography and eluted with a gradient into buffer B (buffer A containing 500 mM imidazole).

Formation and structure determination of the Fab 3G12-RSV $G^{157-197}$ complex. Purified RSV $G^{157-197}$ was mixed in 2-molar excess with purified Fab 3G12, incubated for 1 hour at 4° C, and purified by Superdex 75 size-exclusion chromatography in 10 mM Tris-HCl pH 8.0 and 150 mM NaCl. The Fab 3G12-RSV $G^{157-197}$ complex was concentrated to 15 mg/ml. Crystals were grown by hanging drop vapor diffusion at 22°C with a well solution of 1.8 M Ammonium Sulfate and 100 mM Sodium acetate trihydrate (pH 4.4). Crystals were transferred into a cryoprotectant solution of 2.0 M Ammonium Sulfate, 100 mM Sodium acetate trihydrate (pH 4.4) and 25% glycerol and flash-frozen in liquid nitrogen. Diffraction data were collected at cryogenic temperature at the Advanced Light Source on beamline 8.3.1 using a wavelength of 1.11503 Å. Diffraction data from a single crystal were processed with iMosflm (60) and Aimless (61) (Table 2). The Fab 3G12-RSV $G^{157-197}$ complex structure was solved by molecular replacement with the Fab from PDB 5K59 and the program PHASER (62), and the structure was refined and manually rebuilt using PHENIX (63) and Coot (64), respectively (Table 2).

Expression and purification of RSV G^{ecto}. A synthetic gene encoding RSV G (strain A2) amino acids 64 to 298 (UniProtKB entry P03423) was cloned into pCF in-frame

with an N-terminal TPA signal sequence and Twin-Strep purification tags. Recombinant RSV G^{ecto} was produced by transient-transfection in 293T cells with Fugene HD (Promega, Madison, WI). 6 μg of DNA were transfected with a FuGENE® HD Transfection Reagent:DNA ratio of 3:1. Cell media was supplemented with BioLock (IBA) and 100mM Tris-Cl pH 8.0 and 0.22um-filtered. RSV G^{ecto} proteins were batch purified from media with Strep-Tactin resin (IBA), washed, and eluted with Strep-Tactin elution buffer (100 mM Tris pH 8.0, 150mM NaCl, 1mM EDTA, 2.5mM des-thiobiotin). RSV G^{ecto} proteins were concentrated using a 3kDa spin concentrator.

Chemotaxis assay. The in vitro chemotaxis assay was performed using a Transwell insert plate with an 8-μm pore size, following previously published methods (17, 22, 45). Approximately 2 million log-phase THP-1 cells (a human leukemia monocytic cell line) washed twice and suspended in serum-free RPMI 1640 media were added to the upper chamber of the insert plate. Negative controls were serum-free media alone or serum-free media containing 25 nM bnmAb 3G12 added to the lower chamber. As a positive control, media containing 10% fetal bovine serum (FBS) was added to the lower chamber (data not shown). RSV G^{ecto} was added to the lower chamber at a final concentration of 5 nM in serum-free media. For samples with RSV G^{ecto} and bnmAb 3G12, RSV G^{ecto} was preincubated with 5-molar excess bnmAb for 20 min at room temperature and then added to serum-free media in the lower chamber for a final concentration of 5 nM RSV G^{ecto} and 25 nM bnmAb. The assembled plates were

incubated in a CO_2 incubator at 37°C for 5 hours. Cells migrated to the lower chamber were counted, and the chemotactic indices were determined by comparing the fold increase in cell migration toward the chemoattractant to cell migration toward serum-free media alone. Experiments were performed in three biological replicates.

Accession code. Coordinates and structure factors have been deposited in the Protein Data Bank under accession code 6MKC.

ACKNOWLEDGMENTS

We thank Dr. Sarvind Tripathi for assistance in crystallographic data collection. R.M.D. is supported by the National Institute of Allergy and Infectious Diseases (NIAID) grant R21AI130605. L.M.K. acknowledges partial support from NIAID grant 5R44AI122360-02. This research used resources of the Advanced Light Source (ALS), which is a U.S. Department of Energy (DOE) Office of Science User Facility under contract no. DE-AC02-05CH11231. Beamline 8.3.1 at the Advanced Light Source is operated by the University of California Office of the President, Multicampus Research Programs and Initiatives grant MR-15-328599, the National Institutes of Health (R01 GM124149 and P30 GM124169), Plexxikon Inc.

Table 2. Crystallographic data collection and refinement statistics

	Fab 3G12-RSV $G^{157-197}$
PDB code	6MKC
Data collection[a,b]	
Space group	$P3_12_1$
Cell dimensions	
a, *b*, *c* (Å)	139.33 139.33 94.77
(°)	90.00, 90.00, 120.00
Resolution (Å)	74.53 - 2.90 (3.00 - 2.90)
Total no. reflections	93208 (14475)
No. unique reflections	23682 (3763)
R_{merge}[c]	0.097 (0.641)
I / □□I)	9.4 (1.9)
Completeness (%)	99.5 (99.5)
Redundancy	3.9 (3.8)
$CC_{1/2}$[d]	0.993 (0.601)
Refinement	
Resolution (Å)	74.53 - 2.90
No. reflections	23665
R_{work} / R_{free}[e]	0.1930/ 0.2088
No. atoms	
Protein	3,595
Ligand/ion	0
Water	0
B-factors (Å^2)	
Protein: bnmAb	62.37
Protein: RSV G	76.04
Ligand/ion	0
R.m.s. deviations	
Bond lengths (Å)	0.015
Bond angles (°)	2.067
Ramachandran (%)	
Favored	95.7
Allowed	4.3
Outliers	0

[a] Data from one crystal was used.
[b] Values in parentheses are for highest-resolution shell.
[c] $R_{merge} = \Sigma|(I - \langle I \rangle)| / \Sigma(I)$, where I is the observed intensity.
[d] $CC_{1/2}$ = Pearson correlation coefficient between random half-datasets.
[e] $R_{work} = \Sigma||F_o| - |F_c|| / \Sigma|F_o|$ for all data except 5%, which were used for R_{free} calculation

REFERENCES:

1. Shi T, McAllister DA, O'Brien KL, Simoes EAF, Madhi SA, Gessner BD, Polack FP, Balsells E, Acacio S, Aguayo C, Alassani I, Ali A, Antonio M, Awasthi S, Awori JO, Azziz-Baumgartner E, Baggett HC, Baillie VL, Balmaseda A, Barahona A, Basnet S, Bassat Q, Basualdo W, Bigogo G, Bont L, Breiman RF, Brooks WA, Broor S, Bruce N, Bruden D, Buchy P, Campbell S, Carosone-Link P, Chadha M, Chipeta J, Chou M, Clara W, Cohen C, de Cuellar E, Dang DA, Dash-Yandag B, Deloria-Knoll M, Dherani M, Eap T, Ebruke BE, Echavarria M, de Freitas Lazaro Emediato CC, Fasce RA, Feikin DR, Feng L, et al. 2017. Global, regional, and national disease burden estimates of acute lower respiratory infections due to respiratory syncytial virus in young children in 2015: a systematic review and modelling study. Lancet 390:946-958.
2. Falsey AR, Hennessey PA, Formica MA, Cox C, Walsh EE. 2005. Respiratory syncytial virus infection in elderly and high-risk adults. N Engl J Med 352:1749-1759.
3. Amand C, Tong S, Kieffer A, Kyaw MH. 2018. Healthcare resource use and economic burden attributable to respiratory syncytial virus in the United States: a claims database analysis. BMC Health Services Research 18:294.
4. Anonymous. 1998. Palivizumab, a Humanized Respiratory Syncytial Virus Monoclonal Antibody, Reduces Hospitalization From Respiratory Syncytial Virus Infection in High-risk Infants. Pediatrics 102:531-537.

5. Meissner HC, Kimberlin DW. 2013. RSV immunoprophylaxis: does the benefit justify the cost? Pediatrics 132:915-918.

6. Mazur NI, Higgins D, Nunes MC, Melero JA, Langedijk AC, Horsley N, Buchholz UJ, Openshaw PJ, McLellan JS, Englund JA, Mejias A, Karron RA, Simoes EA, Knezevic I, Ramilo O, Piedra PA, Chu HY, Falsey AR, Nair H, Kragten-Tabatabaie L, Greenough A, Baraldi E, Papadopoulos NG, Vekemans J, Polack FP, Powell M, Satav A, Walsh EE, Stein RT, Graham BS, Bont LJ, Respiratory Syncytial Virus Network F. 2018. The respiratory syncytial virus vaccine landscape: lessons from the graveyard and promising candidates. Lancet Infect Dis 18:e295-e311.

7. McLellan JS, Ray WC, Peeples ME. 2013. Structure and function of respiratory syncytial virus surface glycoproteins. Curr Top Microbiol Immunol 372:83-104.

8. Capella C, Chaiwatpongsakorn S, Gorrell E, Risch ZA, Ye F, Mertz SE, Johnson SM, Moore-Clingenpeel M, Ramilo O, Mejias A, Peeples ME. 2017. Prefusion F, postfusion F, G antibodies and disease severity in infants and young children with acute respiratory syncytial virus infection. J Infect Dis doi:10.1093/infdis/jix489.

9. Ngwuta JO, Chen M, Modjarrad K, Joyce MG, Kanekiyo M, Kumar A, Yassine HM, Moin SM, Killikelly AM, Chuang GY, Druz A, Georgiev IS, Rundlet EJ, Sastry M, Stewart-Jones GB, Yang Y, Zhang B, Nason MC, Capella C, Peeples ME, Ledgerwood JE, McLellan JS, Kwong PD, Graham

BS. 2015. Prefusion F-specific antibodies determine the magnitude of RSV neutralizing activity in human sera. Sci Transl Med 7:309ra162.

10. Teng MN, Whitehead SS, Collins PL. 2001. Contribution of the respiratory syncytial virus G glycoprotein and its secreted and membrane-bound forms to virus replication in vitro and in vivo. Virology 289:283-296.

11. Techaarpornkul S, Barretto N, Peeples ME. 2001. Functional analysis of recombinant respiratory syncytial virus deletion mutants lacking the small hydrophobic and/or attachment glycoprotein gene. J Virol 75:6825-6834.

12. Han J, Takeda K, Wang M, Zeng W, Jia Y, Shiraishi Y, Okamoto M, Dakhama A, Gelfand EW. 2014. Effects of anti-g and anti-f antibodies on airway function after respiratory syncytial virus infection. Am J Respir Cell Mol Biol 51:143-154.

13. Boyoglu-Barnum S, Todd SO, Chirkova T, Barnum TR, Gaston KA, Haynes LM, Tripp RA, Moore ML, Anderson LJ. 2015. An anti-G protein monoclonal antibody treats RSV disease more effectively than an anti-F monoclonal antibody in BALB/c mice. Virology 483:117-125.

14. Boyoglu-Barnum S, Chirkova T, Todd SO, Barnum TR, Gaston KA, Jorquera P, Haynes LM, Tripp RA, Moore ML, Anderson LJ. 2014. Prophylaxis with a respiratory syncytial virus (RSV) anti-G protein monoclonal antibody shifts the adaptive immune response to RSV rA2-line19F infection from Th2 to Th1 in BALB/c mice. J Virol 88:10569-10583.

15. Boyoglu-Barnum S, Gaston KA, Todd SO, Boyoglu C, Chirkova T, Barnum TR, Jorquera P, Haynes LM, Tripp RA, Moore ML, Anderson LJ. 2013. A respiratory syncytial virus (RSV) anti-G protein F(ab')2 monoclonal antibody suppresses mucous production and breathing effort in RSV rA2-line19F-infected BALB/c mice. J Virol 87:10955-10967.

16. Jones HG, Ritschel T, Pascual G, Brakenhoff JPJ, Keogh E, Furmanova-Hollenstein P, Lanckacker E, Wadia JS, Gilman MSA, Williamson RA, Roymans D, van 't Wout AB, Langedijk JP, McLellan JS. 2018. Structural basis for recognition of the central conserved region of RSV G by neutralizing human antibodies. PLoS Pathog 14:e1006935.

17. Lee HJ, Lee JY, Park MH, Kim JY, Chang J. 2017. Monoclonal Antibody against G Glycoprotein Increases Respiratory Syncytial Virus Clearance In Vivo and Prevents Vaccine-Enhanced Diseases. PLoS One 12:e0169139.

18. Miao C, Radu GU, Caidi H, Tripp RA, Anderson LJ, Haynes LM. 2009. Treatment with respiratory syncytial virus G glycoprotein monoclonal antibody or F(ab')2 components mediates reduced pulmonary inflammation in mice. J Gen Virol 90:1119-1123.

19. Radu GU, Caidi H, Miao C, Tripp RA, Anderson LJ, Haynes LM. 2010. Prophylactic treatment with a G glycoprotein monoclonal antibody reduces pulmonary inflammation in respiratory syncytial virus (RSV)-challenged naive and formalin-inactivated RSV-immunized BALB/c mice. J Virol 84:9632-9636.

20. Caidi H, Harcourt JL, Tripp RA, Anderson LJ, Haynes LM. 2012. Combination therapy using monoclonal antibodies against respiratory syncytial virus (RSV) G glycoprotein protects from RSV disease in BALB/c mice. PLoS One 7:e51485.

21. Collarini EJ, Lee FE, Foord O, Park M, Sperinde G, Wu H, Harriman WD, Carroll SF, Ellsworth SL, Anderson LJ, Tripp RA, Walsh EE, Keyt BA, Kauvar LM. 2009. Potent high-affinity antibodies for treatment and prophylaxis of respiratory syncytial virus derived from B cells of infected patients. J Immunol 183:6338-6345.

22. Tripp RA, Power UF, Openshaw PJM, Kauvar LM. 2018. Respiratory Syncytial Virus: Targeting the G Protein Provides a New Approach for an Old Problem. J Virol 92.

23. Satake M, Coligan JE, Elango N, Norrby E, Venkatesan S. 1985. Respiratory syncytial virus envelope glycoprotein (G) has a novel structure. Nucleic Acids Res 13:7795-7812.

24. Wertz GW, Collins PL, Huang Y, Gruber C, Levine S, Ball LA. 1985. Nucleotide sequence of the G protein gene of human respiratory syncytial virus reveals an unusual type of viral membrane protein. Proc Natl Acad Sci U S A 82:4075-4079.

25. Johnson SM, McNally BA, Ioannidis I, Flano E, Teng MN, Oomens AG, Walsh EE, Peeples ME. 2015. Respiratory Syncytial Virus Uses CX3CR1 as a

Receptor on Primary Human Airway Epithelial Cultures. PLoS Pathog 11:e1005318.

26. Tripp RA, Jones LP, Haynes LM, Zheng H, Murphy PM, Anderson LJ. 2001. CX3C chemokine mimicry by respiratory syncytial virus G glycoprotein. Nat Immunol 2:732-738.

27. Chirkova T, Lin S, Oomens AG, Gaston KA, Boyoglu-Barnum S, Meng J, Stobart CC, Cotton CU, Hartert TV, Moore ML, Ziady AG, Anderson LJ. 2015. CX3CR1 is an important surface molecule for respiratory syncytial virus infection in human airway epithelial cells. J Gen Virol 96:2543-2556.

28. Jeong KI, Piepenhagen PA, Kishko M, DiNapoli JM, Groppo RP, Zhang L, Almond J, Kleanthous H, Delagrave S, Parrington M. 2015. CX3CR1 Is Expressed in Differentiated Human Ciliated Airway Cells and Co-Localizes with Respiratory Syncytial Virus on Cilia in a G Protein-Dependent Manner. PLoS One 10:e0130517.

29. Bukreyev A, Yang L, Fricke J, Cheng L, Ward JM, Murphy BR, Collins PL. 2008. The secreted form of respiratory syncytial virus G glycoprotein helps the virus evade antibody-mediated restriction of replication by acting as an antigen decoy and through effects on Fc receptor-bearing leukocytes. J Virol 82:12191-12204.

30. Chirkova T, Boyoglu-Barnum S, Gaston KA, Malik FM, Trau SP, Oomens AG, Anderson LJ. 2013. Respiratory syncytial virus G protein CX3C motif

impairs human airway epithelial and immune cell responses. J Virol 87:13466-13479.

31. Harcourt J, Alvarez R, Jones LP, Henderson C, Anderson LJ, Tripp RA. 2006. Respiratory syncytial virus G protein and G protein CX3C motif adversely affect CX3CR1+ T cell responses. J Immunol 176:1600-1608.

32. Arnold R, Konig B, Werchau H, Konig W. 2004. Respiratory syncytial virus deficient in soluble G protein induced an increased proinflammatory response in human lung epithelial cells. Virology 330:384-397.

33. Haynes LM, Jones LP, Barskey A, Anderson LJ, Tripp RA. 2003. Enhanced disease and pulmonary eosinophilia associated with formalin-inactivated respiratory syncytial virus vaccination are linked to G glycoprotein CX3C-CX3CR1 interaction and expression of substance P. J Virol 77:9831-9844.

34. Sugawara M, Czaplicki J, Ferrage J, Haeuw JF, Power UF, Corvaia N, Nguyen T, Beck A, Milton A. 2002. Structure-antigenicity relationship studies of the central conserved region of human respiratory syncytial virus protein G. J Pept Res 60:271-282.

35. Langedijk JP, de Groot BL, Berendsen HJ, van Oirschot JT. 1998. Structural homology of the central conserved region of the attachment protein G of respiratory syncytial virus with the fourth subdomain of 55-kDa tumor necrosis factor receptor. Virology 243:293-302.

36. Doreleijers JF, Langedijk JP, Hard K, Boelens R, Rullmann JA, Schaaper WM, van Oirschot JT, Kaptein R. 1996. Solution structure of the

immunodominant region of protein G of bovine respiratory syncytial virus. Biochemistry 35:14684-14688.

37. Feldman SA, Hendry RM, Beeler JA. 1999. Identification of a linear heparin binding domain for human respiratory syncytial virus attachment glycoprotein G. J Virol 73:6610-6617.

38. Hallak LK, Collins PL, Knudson W, Peeples ME. 2000. Iduronic acid-containing glycosaminoglycans on target cells are required for efficient respiratory syncytial virus infection. Virology 271:264-275.

39. Cortjens B, Yasuda E, Yu X, Wagner K, Claassen YB, Bakker AQ, van Woensel JBM, Beaumont T. 2017. Broadly Reactive Anti-Respiratory Syncytial Virus G Antibodies from Exposed Individuals Effectively Inhibit Infection of Primary Airway Epithelial Cells. J Virol 91.

40. Lee J, Klenow L, Coyle EM, Golding H, Khurana S. 2018. Protective antigenic sites in respiratory syncytial virus G attachment protein outside the central conserved and cysteine noose domains. PLoS Pathog 14:e1007262.

41. Haynes LM, Caidi H, Radu GU, Miao C, Harcourt JL, Tripp RA, Anderson LJ. 2009. Therapeutic monoclonal antibody treatment targeting respiratory syncytial virus (RSV) G protein mediates viral clearance and reduces the pathogenesis of RSV infection in BALB/c mice. J Infect Dis 200:439-447.

42. Boyoglu-Barnum S, Todd SO, Meng J, Barnum TR, Chirkova T, Haynes LM, Jadhao SJ, Tripp RA, Oomens AG, Moore ML, Anderson LJ. 2017. Mutating

the CX3C motif in the G protein should make a live respiratory syncytial virus vaccine safer and more effective. J Virol doi:10.1128/JVI.02059-16.

43. Shingai M, Azuma M, Ebihara T, Sasai M, Funami K, Ayata M, Ogura H, Tsutsumi H, Matsumoto M, Seya T. 2008. Soluble G protein of respiratory syncytial virus inhibits Toll-like receptor 3/4-mediated IFN-beta induction. Int Immunol 20:1169-1180.

44. Kauvar LM, A Collarini EJ, A Keyt B, A Foord O. 2010. Anti-RSV G protein antibodies. Patent number US 8273354.

45. Fedechkin SO, George NL, Wolff JT, Kauvar LM, DuBois RM. 2018. Structures of Respiratory Syncytial Virus G Antigen Bound to Broadly-Neutralizing Antibodies. Science Immunology In press.

46. Escribano-Romero E, Rawling J, Garcia-Barreno B, Melero JA. 2004. The soluble form of human respiratory syncytial virus attachment protein differs from the membrane-bound form in its oligomeric state but is still capable of binding to cell surface proteoglycans. J Virol 78:3524-3532.

47. Fuentes S, Coyle EM, Golding H, Khurana S. 2015. Nonglycosylated G-Protein Vaccine Protects against Homologous and Heterologous Respiratory Syncytial Virus (RSV) Challenge, while Glycosylated G Enhances RSV Lung Pathology and Cytokine Levels. J Virol 89:8193-8205.

48. Cullen LM, Schmidt MR, Morrison TG. 2017. The importance of RSV F protein conformation in VLPs in stimulation of neutralizing antibody titers in mice previously infected with RSV. Hum Vaccin Immunother 13:2814-2823.

49. de Taeye SW, de la Pena AT, Vecchione A, Scutigliani E, Sliepen K, Burger JA, van der Woude P, Schorcht A, Schermer EE, van Gils MJ, LaBranche CC, Montefiori DC, Wilson IA, Moore JP, Ward AB, Sanders RW. 2018. Stabilization of the gp120 V3 loop through hydrophobic interactions reduces the immunodominant V3-directed non-neutralizing response to HIV-1 envelope trimers. J Biol Chem 293:1688-1701.

50. Krammer F, Pica N, Hai R, Tan GS, Palese P. 2012. Hemagglutinin Stalk-Reactive Antibodies Are Boosted following Sequential Infection with Seasonal and Pandemic H1N1 Influenza Virus in Mice. J Virol 86:10302-10307.

51. Hai R, Krammer F, Tan GS, Pica N, Eggink D, Maamary J, Margine I, Albrecht RA, Palese P. 2012. Influenza viruses expressing chimeric hemagglutinins: globular head and stalk domains derived from different subtypes. J Virol 86:5774-5781.

52. Krammer F, Pica N, Hai R, Margine I, Palese P. 2013. Chimeric hemagglutinin influenza virus vaccine constructs elicit broadly protective stalk-specific antibodies. J Virol 87:6542-6550.

53. Impagliazzo A, Milder F, Kuipers H, Wagner MV, Zhu X, Hoffman RM, van Meersbergen R, Huizingh J, Wanningen P, Verspuij J, de Man M, Ding Z, Apetri A, Kukrer B, Sneekes-Vriese E, Tomkiewicz D, Laursen NS, Lee PS, Zakrzewska A, Dekking L, Tolboom J, Tettero L, van Meerten S, Yu W, Koudstaal W, Goudsmit J, Ward AB, Meijberg W, Wilson IA, Radosevic K.

2015. A stable trimeric influenza hemagglutinin stem as a broadly protective immunogen. Science 349:1301-1306.

54. Lu Y, Welsh JP, Swartz JR. 2014. Production and stabilization of the trimeric influenza hemagglutinin stem domain for potentially broadly protective influenza vaccines. Proc Natl Acad Sci U S A 111:125-130.

55. Pallesen J, Wang N, Corbett KS, Wrapp D, Kirchdoerfer RN, Turner HL, Cottrell CA, Becker MM, Wang L, Shi W, Kong WP, Andres EL, Kettenbach AN, Denison MR, Chappell JD, Graham BS, Ward AB, McLellan JS. 2017. Immunogenicity and structures of a rationally designed prefusion MERS-CoV spike antigen. Proc Natl Acad Sci U S A 114:E7348-E7357.

56. Stewart-Jones GBE, Chuang GY, Xu K, Zhou T, Acharya P, Tsybovsky Y, Ou L, Zhang B, Fernandez-Rodriguez B, Gilardi V, Silacci-Fregni C, Beltramello M, Baxa U, Druz A, Kong WP, Thomas PV, Yang Y, Foulds KE, Todd JP, Wei H, Salazar AM, Scorpio DG, Carragher B, Potter CS, Corti D, Mascola JR, Lanzavecchia A, Kwong PD. 2018. Structure-based design of a quadrivalent fusion glycoprotein vaccine for human parainfluenza virus types 1-4. Proc Natl Acad Sci U S A 115:12265-12270.

57. McLellan JS, Chen M, Joyce MG, Sastry M, Stewart-Jones GB, Yang Y, Zhang B, Chen L, Srivatsan S, Zheng A, Zhou T, Graepel KW, Kumar A, Moin S, Boyington JC, Chuang GY, Soto C, Baxa U, Bakker AQ, Spits H, Beaumont T, Zheng Z, Xia N, Ko SY, Todd JP, Rao S, Graham BS, Kwong

PD. 2013. Structure-based design of a fusion glycoprotein vaccine for respiratory syncytial virus. Science 342:592-598.

58. Chu HM, Wright J, Chan YH, Lin CJ, Chang TW, Lim C. 2014. Two potential therapeutic antibodies bind to a peptide segment of membrane-bound IgE in different conformations. Nat Commun 5:3139.

59. Deng L, Ma L, Virata-Theimer ML, Zhong L, Yan H, Zhao Z, Struble E, Feinstone S, Alter H, Zhang P. 2014. Discrete conformations of epitope II on the hepatitis C virus E2 protein for antibody-mediated neutralization and nonneutralization. Proc Natl Acad Sci U S A 111:10690-10695.

60. Battye TG, Kontogiannis L, Johnson O, Powell HR, Leslie AG. 2011. iMOSFLM: a new graphical interface for diffraction-image processing with MOSFLM. Acta Crystallogr D Biol Crystallogr 67:271-281.

61. Evans PR, Murshudov GN. 2013. How good are my data and what is the resolution? Acta Crystallogr D Biol Crystallogr 69:1204-1214.

62. McCoy AJ, Grosse-Kunstleve RW, Adams PD, Winn MD, Storoni LC, Read RJ. 2007. Phaser crystallographic software. J Appl Crystallogr 40:658-674.

63. Adams PD, Afonine PV, Bunkoczi G, Chen VB, Davis IW, Echols N, Headd JJ, Hung LW, Kapral GJ, Grosse-Kunstleve RW, McCoy AJ, Moriarty NW, Oeffner R, Read RJ, Richardson DC, Richardson JS, Terwilliger TC, Zwart PH. 2010. PHENIX: a comprehensive Python-based system for macromolecular structure solution. Acta Crystallogr D Biol Crystallogr 66:213-221.

64. Emsley P, Cowtan K. 2004. Coot: model-building tools for molecular graphics. Acta Crystallogr D Biol Crystallogr 60:2126-2132.

Appendix I

Structural characterization of human astrovirus acidic domain

N-terminal GST-tagged Acidic Domain Helices construct (ADH) was set up in crystal trials (Figure II, Figure III, Figure IV). The construct did not crystallize. Produced spherulites but no diffraction after optimization of solutions (Figure V). N-terminal 6xHis tag and Gb1 tagged ADH was set up in crystal trials, produced birefringent phase separation, but did not diffract (Figure V). No other crystal hits were observed, and optimization did not produce diffracting crystals.

GST-ADH was prescission protease cleaved, however ADH bound to GST and did not separate (Figure III). Attempted sizing chromatography, ion exchange chromatography, high salt, DTT, glycerol, buffers and pH, did not separate GST from ADH post prescission protease cleavage.

Expressed full length HAstV-1 C-terminal acidic domain, trypsinized to isolate folded 10 kDa fragment (Figure IV). Fragment eluted in void volume, indicative of a disordered region. The isolated 15 kDa fragment degrades into 10 kDa fragment overtime, occurs overnight at 37° C or in ~1week at 4° C.

Set up crystal trials with isolated and purified 10 kDa acidic domain protein post-trypsin (Figure V). Crystal trials produced spherulites, amorphous separation, microcrystalline phase separation. None of these were diffracting. Attempted

expansion grid and seeding, both self-seeding and cross-seeding, did not improve hits or produce diffraction.

Expressed acidic domain helices construct with an N-terminal 6xHis tag and Gb1 solubility tag (Figure VI). After TEV cleavage and purifcation, ADH did not separate from Gb1. Puried intact pHisGb1-ADH sample by size exclusion and ion exchange chromatography and set up in crystal trials (Figure VII).

Ran N^{15} labelled C-terminal acidic domain on size exclusion chromatography (S200), and isolated pure, homogeneous sample (Figure VIII). Performed circular dichroism, 60-65% random coil (unstructured) and 35-40% helical, distinct minima at 222nm and 208 nm (Fig 3.8).

Trypsinized C-terminal acidic domain, isolated a 10kDa and 5kDa fragments, purified on S200 (Figure IX). Ran HSQC, sample is disordered, broad peaks, clustered around 8-8.5ppm (Figure XII) (Figure XII).

Table 3. Human astrovirus-1acidic domain list of plasmids and construct descriptions.

Plasmid	Description
pET52b_HAstV-1_Capsid_CAD_helices	C-term. 6xHis tag acidic domain helices construct (res. 292-380)
pET52b_HAstV-1_Capsid_CAD	C-term. 6xHis tag full length acidic domain (res 239-380)
pGEX6p-3_HAstV-1_Capsid_CAD_helices_Gibson	N-term. GST-tag (res. 292-380)
pHisGB1_ADH	N-term. 6xHis Gb1 acidic domain helices construct (res. 292-380)

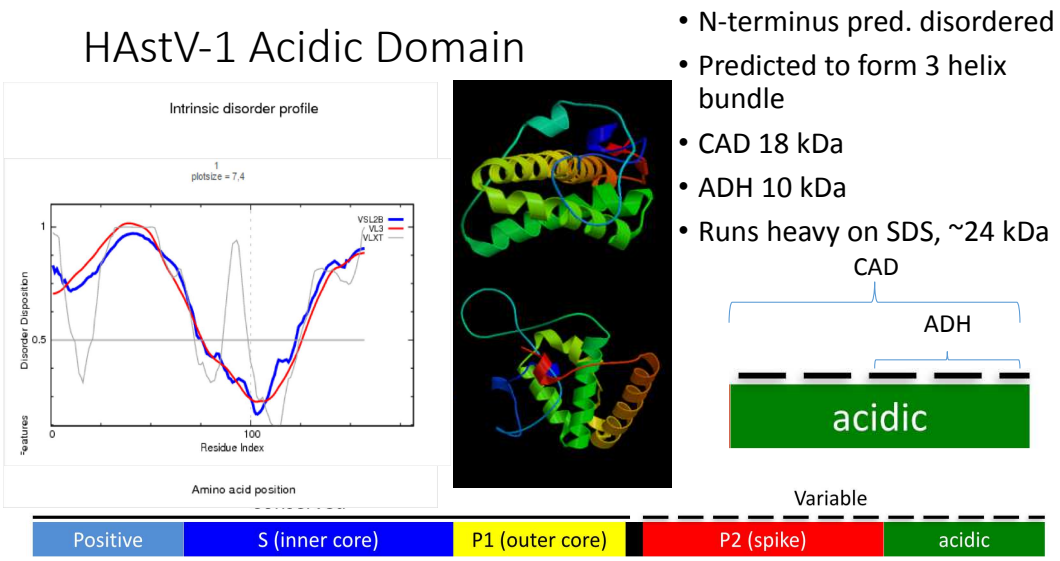

Figure I. Human astrovirus acidic domain project overview.

Left: PSIPRED prediction of disorder, the acidic domain is largely predicted to be disordered with a short helical region. Middle: Rosetta prediction for acidic domain, showing three helices, agreeing with PSIPRED and other secondary structure predictions. Bottom: schematic overview of human astrovirus capsid domains.

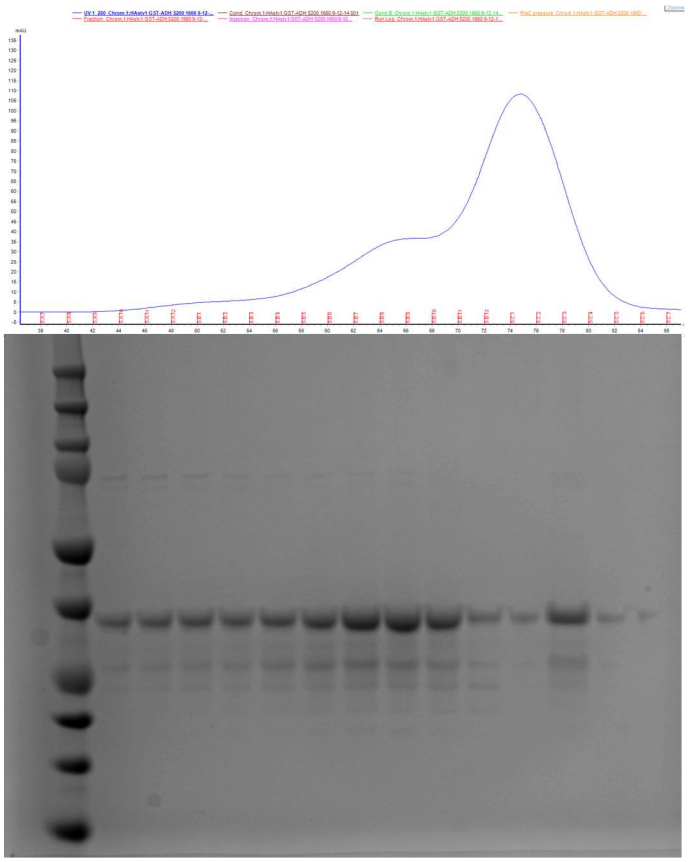

Figure II. GST-acidic domain helices sizing purification. Top, GST-Acidic domain helices S75 purification. Bottom gel showing purity for sample set up in crystal trials.

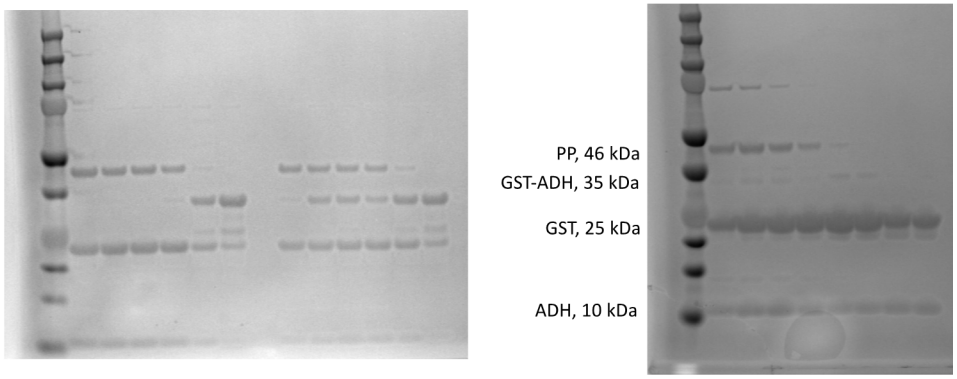

Figure III. Left: GST-ADH prescission protease cleavage trial. Right, GST-ADH.

Precission protease cleavage with optimized temperature, time, and buffer conditions.

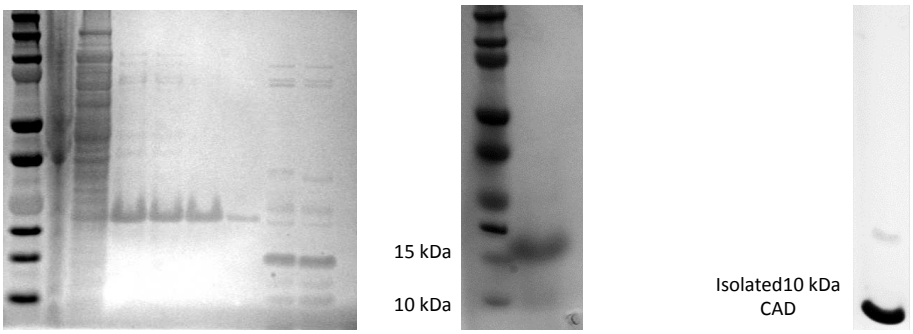

Figure IV. HAstV-1 C-terminal acidic domain expression and trypsin digest.

Left, expression and TALON purification. Middle, isolation of 15 kDa and 10 kDa band after trypsin digest. Right: degradation of 15 kDa protein into 10 kDa overtime; occurs overnight at 37° C or in ~1week at 4° C.

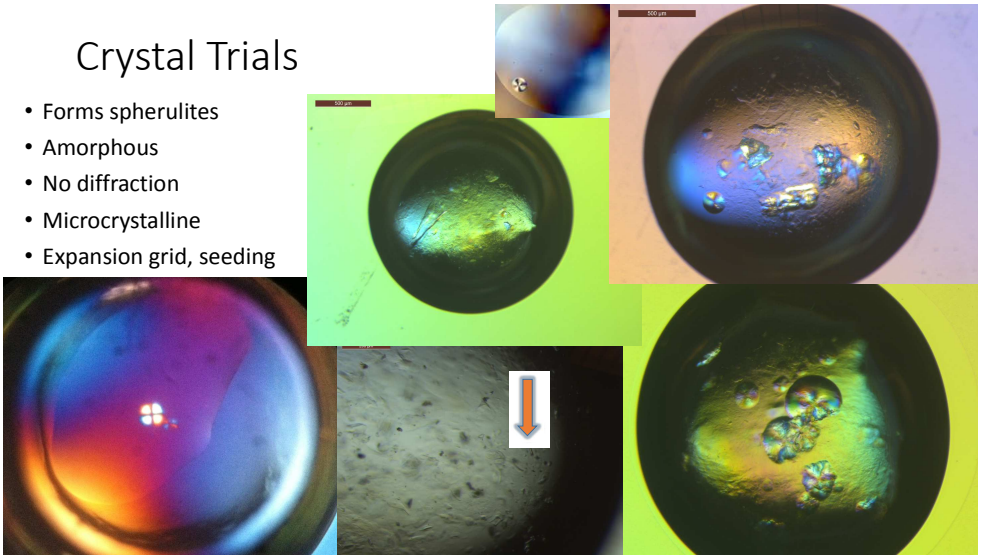

Figure V. C-terminal acidic domain 10 kDa product crystal trials.

Representative spehrulites, birefringent phase separation, amorphous phase separation and other activity in drops. None of these produced diffraction.

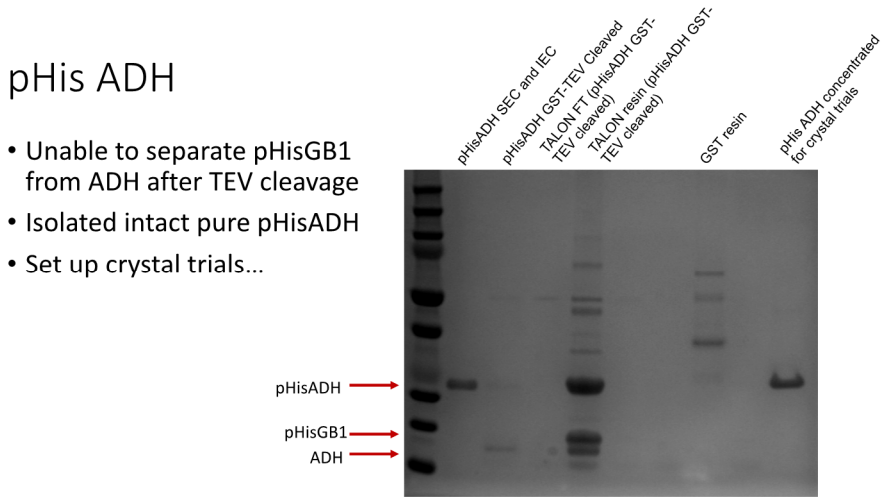

Figure VI. pHisGb1 Acidic domain helices construct expression, purification and

TEV digest.

After TEV digest, ADH bound to Gb1, isolated and purified intact pHisGb1-ADH construct for crystal trials

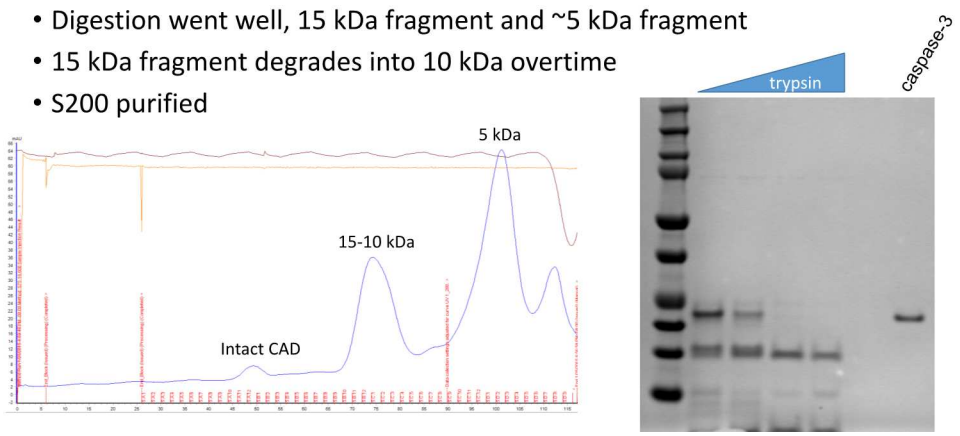

Figure VII. Trypsin digest and caspase-3 digest of intact C-terminal acidic domain construct.

Isolated a 15 kDa fragment and a 5 kDa fragment.

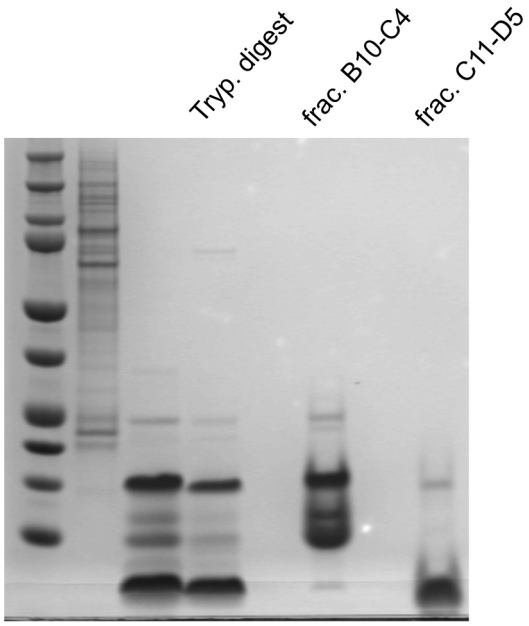

Figure VIII. Large scale trypsin digest of ^{15}N labelled CAD NMR sample to isolate

15 kDa and 10 kDa fragments.

Purified the trypsin digested samples on size exclusion chromatography and separated the15 kDa and 10 kDa fragments.

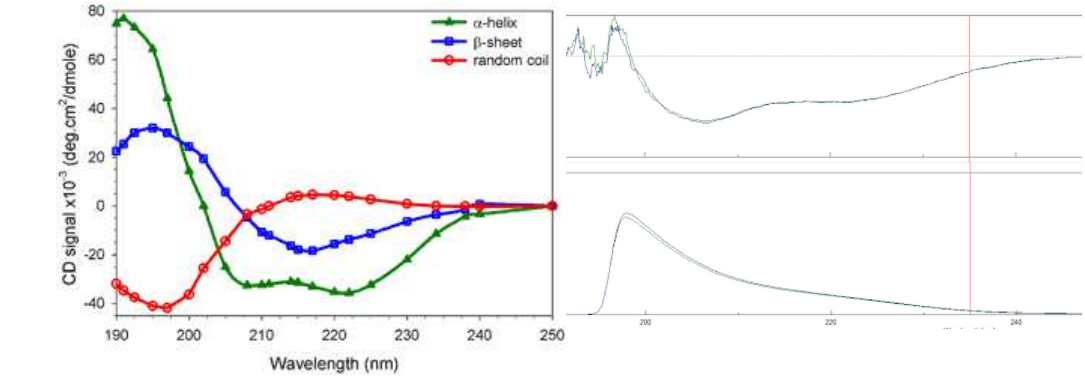

Figure IX Circular dichroism spectra of C-terminal acidic domain.

Left, representative circular dichroism spectra of various secondary structures. Right, CAD is ~60-65% unstructured and 35-40% helical. Distinct minima are visible at 222nm and 208nm.

15N CAD Expression and Purification

- Isolate full length acidic for NMR experiments
- Anion Exchange

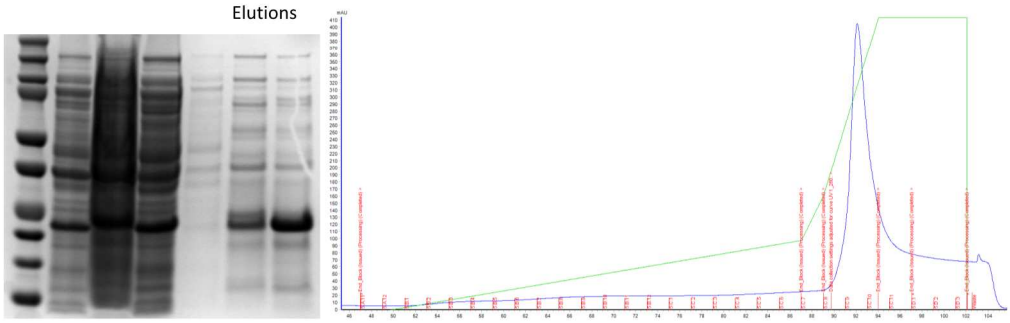

Figure X. ^{15}N labelled C-terminal acidic domain expression and purification on ion exchange.

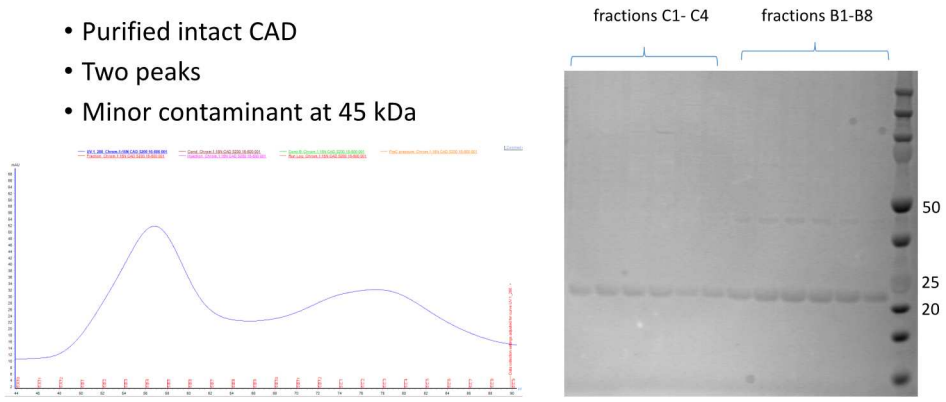

Figure XI. C-terminal acidic domain ^{15}N labelled for NMR studies.

Isolated mostly pure full length CAD after S200 sizing purification for NMR studies.

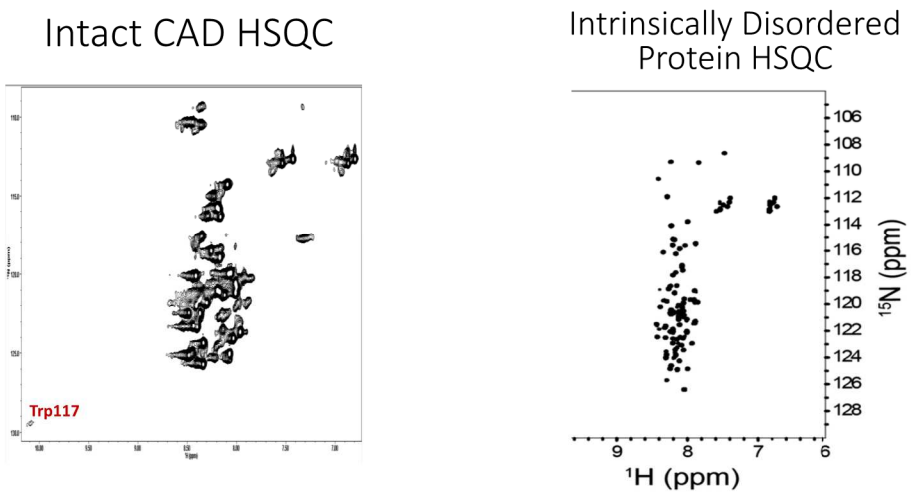

Figure XII. HSQC spectrum of full length C-terminal acidic domain.

Left: Full length C-terminal acidic domain HSQC. Right: representative HSQC of a disordered protein.

Appendix II

Human astrovirus PS spike and capsid

Goal: to determine the structure of Human astrovirus PS spike domain. Due to low sequence conservation and no clear domain boundaries past the core domain of astrovirus PS capsid, it's difficult to identify where the domain boundaries for PS spike start and end (Figure XXX). The capsid N-terminus is strongly predicted to be disorder as is the large portion of the C-terminal acidic domain (Figure XIII). The core domain and spike domain region of the capsid is predicted to be mostly ordered, with short, sharp spikes indicative of loops and other flexible regions common in structured domains (Figure XIII). In order to determine the PS spike domain sequence, full length PS capsid was expressed and several digestion approaches and MS techniques used to isolate and identify the spike construct.

Expressed HAstV-PS full length capsid in Sf9 cells, purified by TALON and isolated a full length HAstV-PS capsid band at 88kDa (Figure XXIX). Trypsin digested the sample and a new 25kDa appeared (Figure XXXI). Performed in gel trypsin digest and mass spec to identify band, exact mass of band is 25,954 Da and based on trypsin digest potential constructs that would match the mass within the HAstV-PS capsid are as follows: 351-581, 271-506, 292-526 (Figure XXXI Figure XXXII).

For PS-spike project, tried expressing the following constructs: PS1 394-655, PS2 394-737, PS3 394-615, PS4 394-660, PS5 res. 394-653, PS6 417-645, PS7 394-680, PS8 394-645, PS9 433-678, PS10 417-640, PS11 417-689, PS12 417-678 (Figure XIV, Figure XV, Figure XVI, Figure XVII, Figure XVIII, Figure XIX, Figure XX, Figure XXI, Figure XXII, Figure XXIII, Figure XXIV, Figure XXV, Figure XXVI, Figure XXVII, Figure XXVIII, Figure XXIX). Expressed constructs with 6xHis tag, pHisGb1 solubility tag and GST tag. Most constructs did not express, expressed poorly or insolubly. Adding solubility tags such as GST and Gb1 helped with solubility, but most constructs degraded after expression (Figure XXIX).

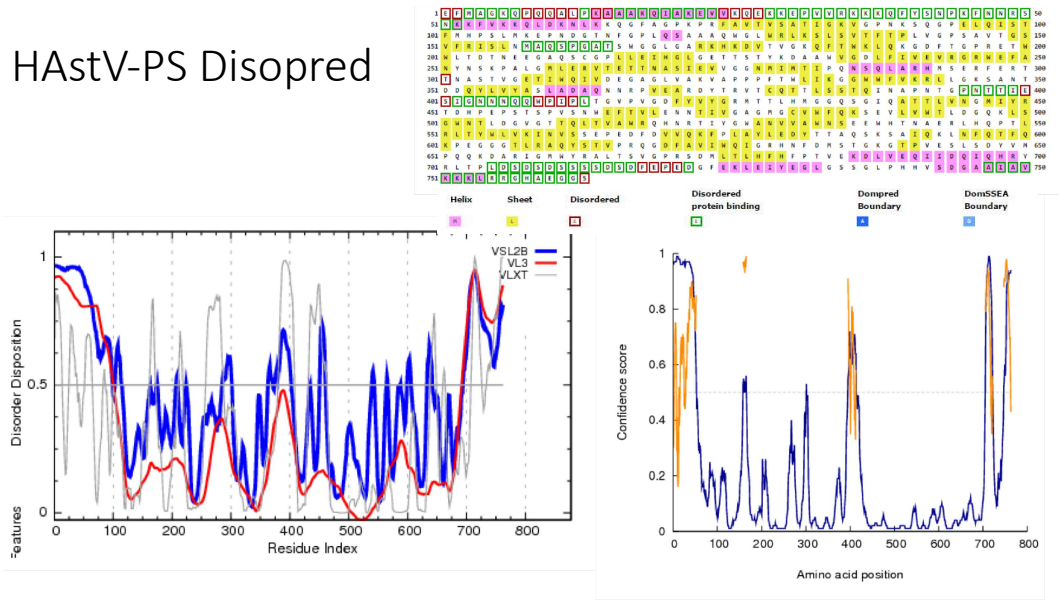

Figure XIII. Disorder and secondary structure prediction for human astrovirus PS capsid.

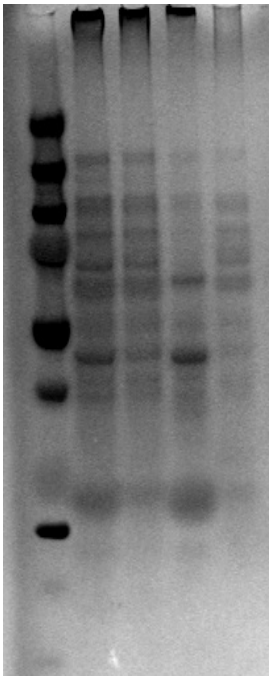

Figure XIV. GST-PS2 expression and TEV cleavage.

GST-PS2 is contaminated after GST purification and did not separate after TEV cleavage and flowthrough.

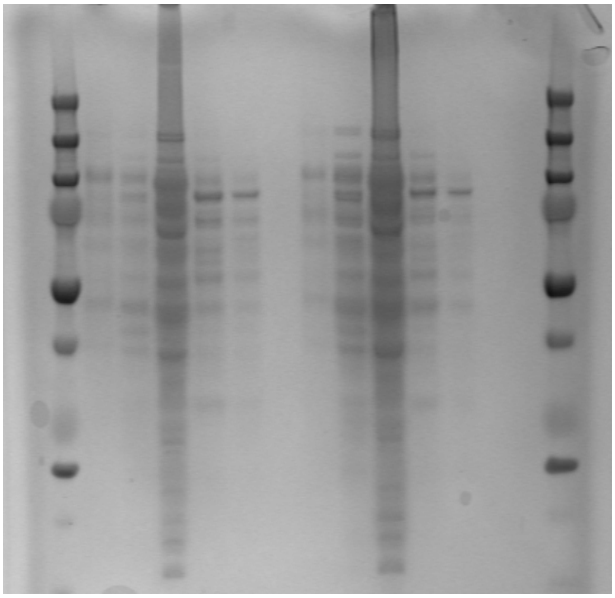

Figure XV. pET52b PS3 and pET52b PS4 expression and purification with TALON.

Lane order, 1. Ladder, 2. Culture PS3, 3. lysate PS3, 4. pellet PS3, 5. TALON elution PS3, 6. TALON elution 2 PS3. 7. 8. Culture PS4, 9. lysate PS4, 10. pellet PS4, 11. TALON elution PS4, 6. TALON elution 2 PS4. Samples are heavily contaminated and poorly expressed.

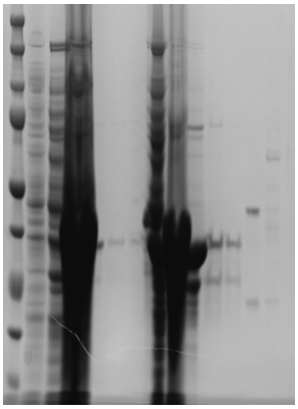

Figure XVI. GST-PS2 PreScission protease (PP) cleavage and purification.

PS2 did not separate from PP after cleavage and purification (lane 14 and 15)

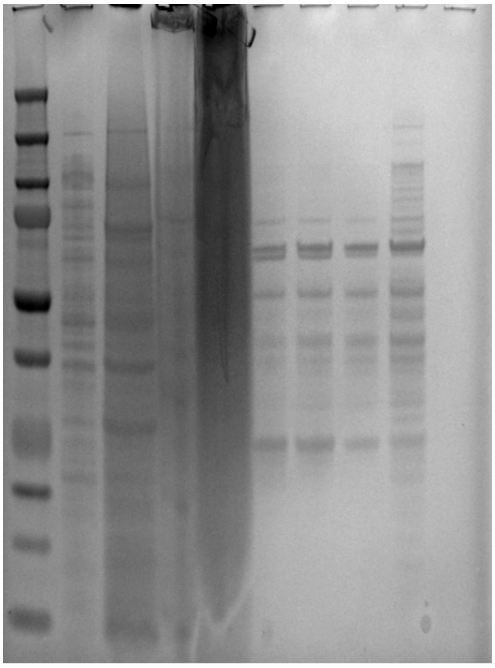

Figure XVII. GST-PS2 expression and GST purification.

1. MW Ladder 2. pre-IPTG 3. BL21 lysate 4. pellet 5. FT (after binding GST resin) 6. E1 7. E2 8. E3 9. E4 (added 5mM DTT in elution buffer) 10.

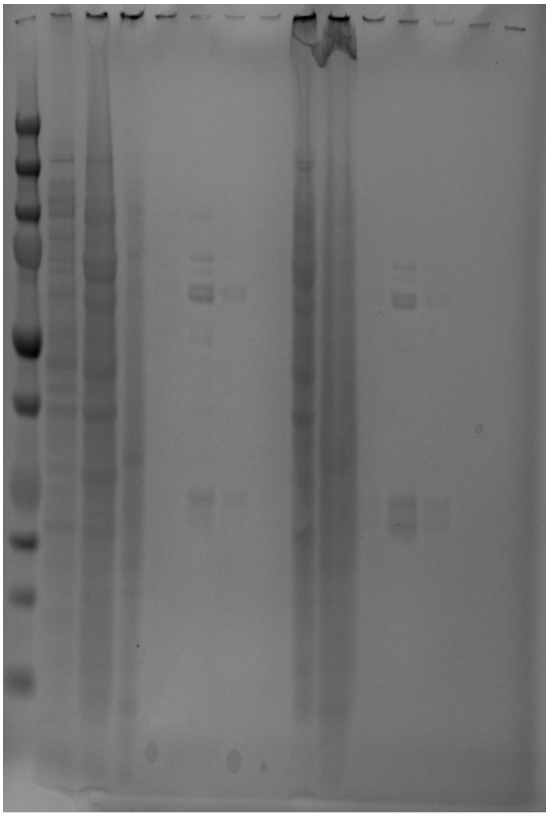

Figure XVIII. GST-PS1 and GST-PS2 expression.

Lanes 6-7, GST-PS1 elutions after expression and GST purificaiton. Lanes 12-13, GST-PS2 elutions after expression and GST purification.

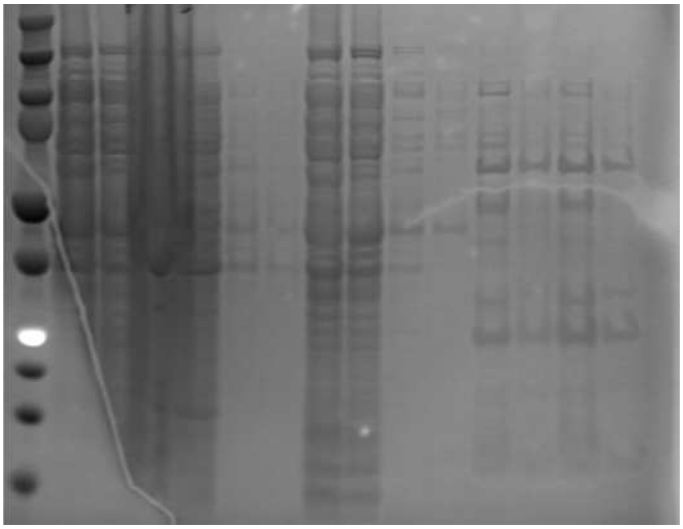

Figure XIX. pHisGb1 PS3 and pET52b His tagged PS3 expression.

Both samples expressed but had heavy contamination post purification. Lane description: 1. MW Ladder 2. pHisGB1 PS3 lysate 3. pET52b PS3 lysate 4. pHisGB1 PS3 pellet 5. pET52bPS3 pellet 6. pHisGB1 PS3 pre-IPTG 7. pET52bPS3 pre-IPTG 8. pHisGB1 PS3 FT 9. pET52bPS3 FT 10. pHisGB1 PS3 W1 11. pET52bPS3 W1 12. pHisGB1 PS3 E1 13. pET52b PS3 E1 14. pHisGB1 PS3 E2 15. pET52b PS3 E2

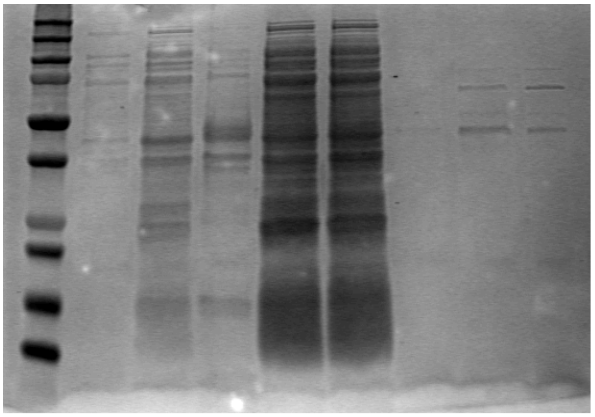

Figure XX. HAstV-PS C4 construct, expression and purification.

Expression looks moderate and yields were low after purification and sample was not pure.

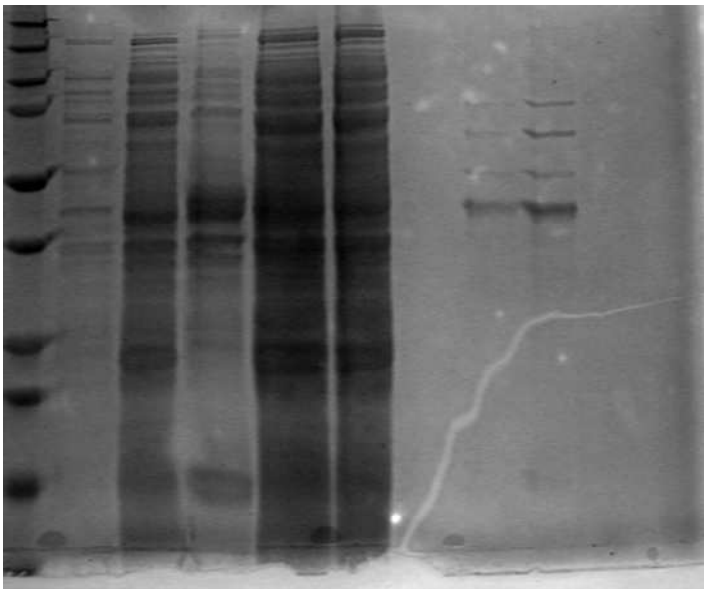

Figure XXI. HAstV-PS PS5 construct, expression and purification.

Expression looks moderate and yields were low after purification and sample was not pure.

C6

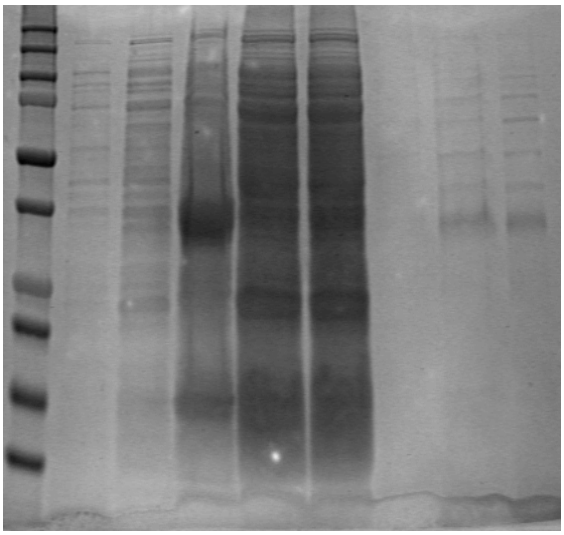

Figure XXII. HAstV-PS PS6 construct, expression and purification.

Expression looks moderate and yields were low after purification and sample was not pure.

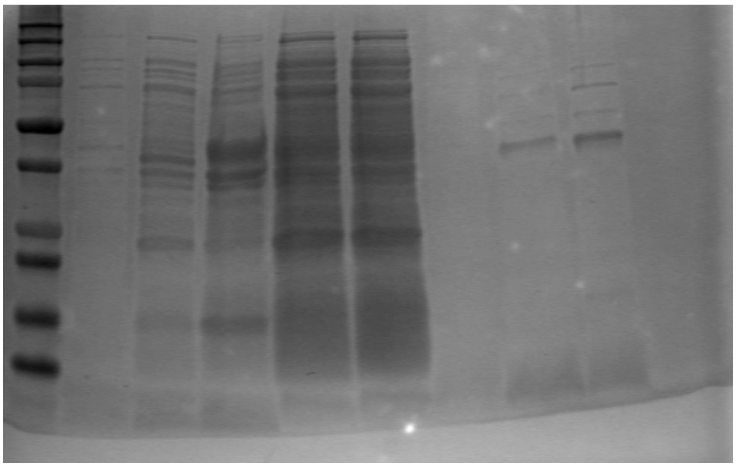

Figure XXIII. HAstV-PS PS8 construct, expression and purification.

Expression looks moderate and yields were low after purification and sample was not pure.

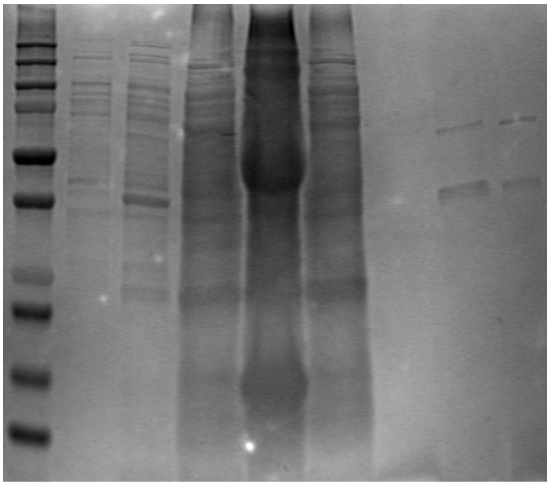

Figure XXIV. HAstV-PS PS9 construct, expression and purification.

Expression looks moderate and yields were low after purification and sample was not pure.

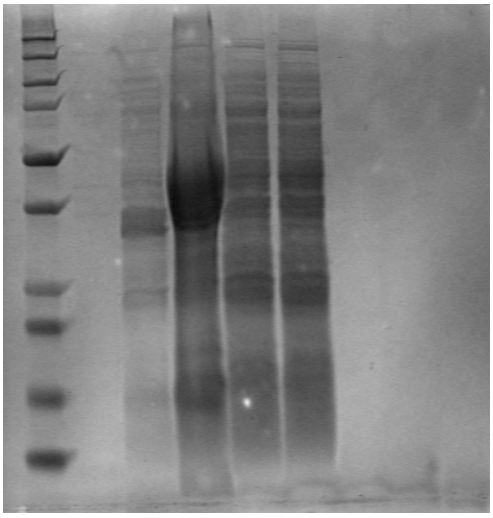

Figure XXV. HAstV-PS PS10 construct, expression and purification.

Expression looks moderate and yields were low after purification and sample was not pure.

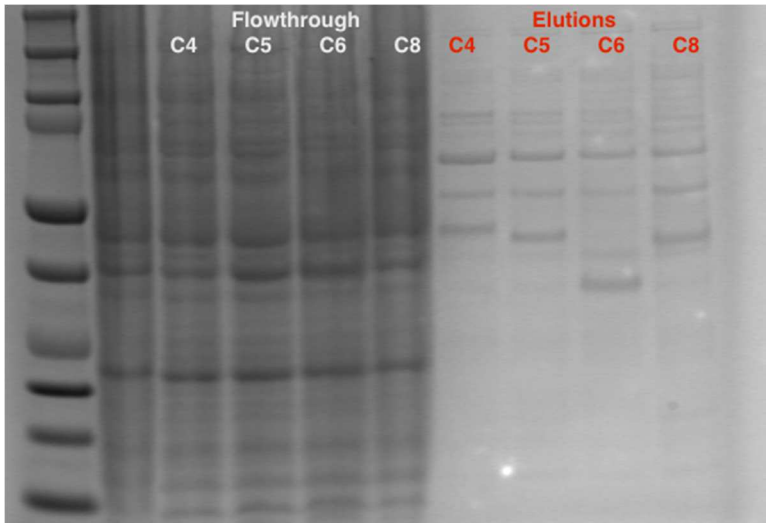

Figure XXVI. Expression and purification of HAstV PS4, PS5, PS6, and PS8 constructs.

All constructs expressed at moderate level and had significant contamination after TALON purification.

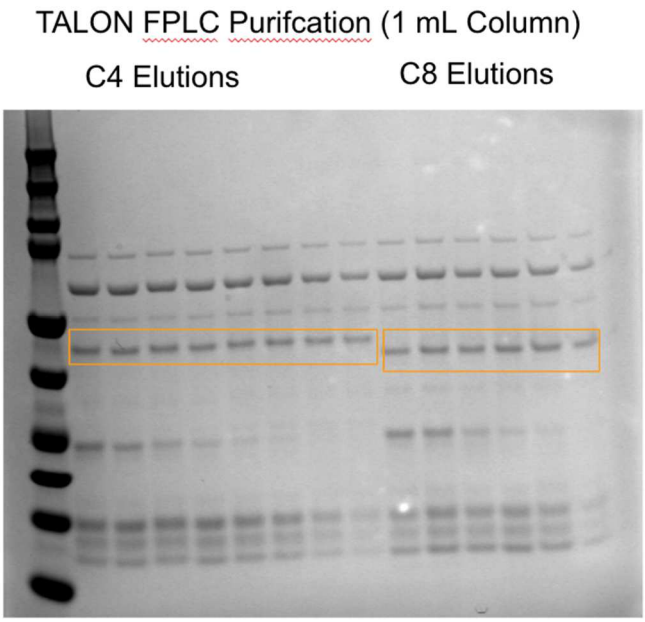

Figure XXVII. TALON purification of HAstV PS4 and PS8 constructs.

Both PS4 and PS8 samples had major contamination after performing TALON purification on FPLC.

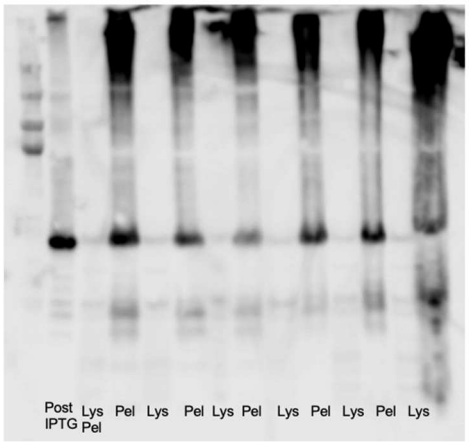

Figure XXVIII. Representative Western Blot of C4 C8 constructs expressed in E.coli.

Most of the protein is in the pellet with a very small amount in the soluble fraction of lysate. Optimizing expression and purification did not improve yields.

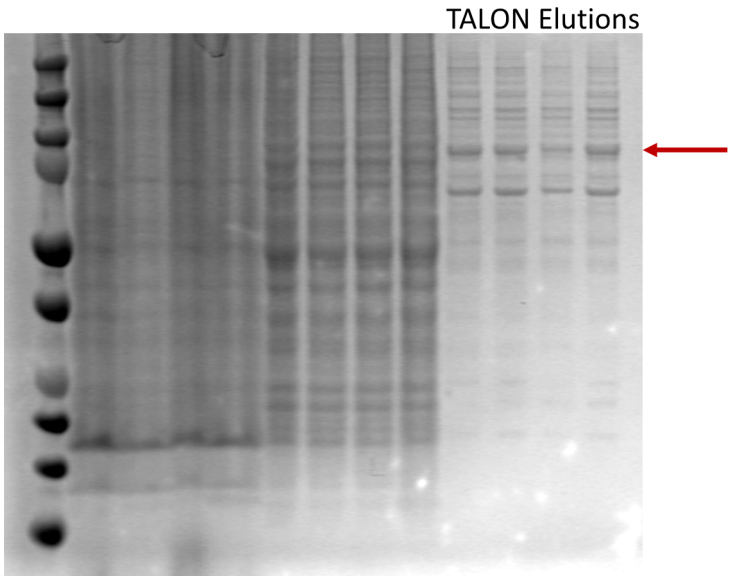

Figure XXIX. HAstV-PS capsid expression in Sf9 cells.

Expression, TALON purification. Degradation bands are visible in the TALON elution .

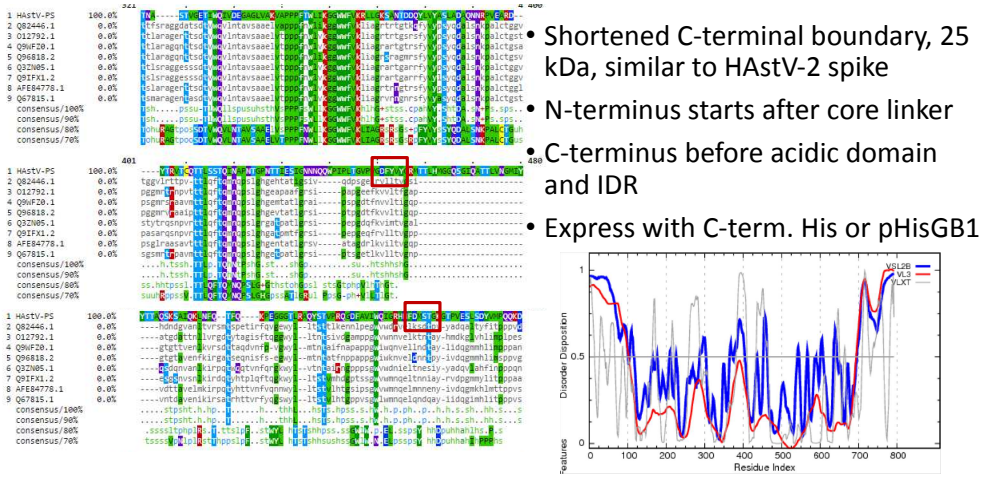

Figure XXX. Alignment of PS capsid spike sequences.

Rationale for designing constructs past PS1 and PS2. For PS3 res. 425-635 were chosen based on molecular weight, 25 kDa, which is close to the molecular weight HAstV-1 spike. The N-terminus starts after the predicted disordered core linker sequence and the C-terminus ends before acidic predicted intrinsically disordered region.

HAstV-PS Trypsinized

- Intact capsid at 88 kDa disappears as trypsin conc. ↑
- Native 25 kDa band disappears as trypsin conc. ↑
- Too small for core domain (~37 kDa)
- Smaller band appears
- PS spike?

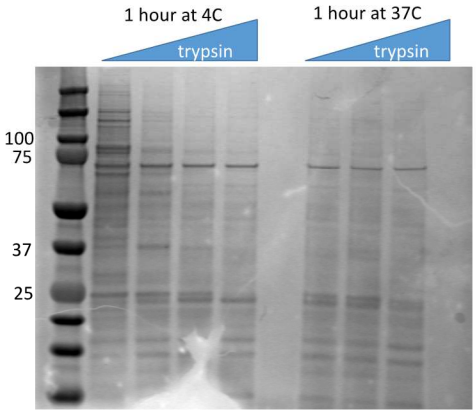

Figure XXXI. Human astrovirus PS full length capsid trypsin digest.

As trypsin concentration increases 88 kDa full length capsid band disappears and a 25 kDa and 37 kDa bands appear.

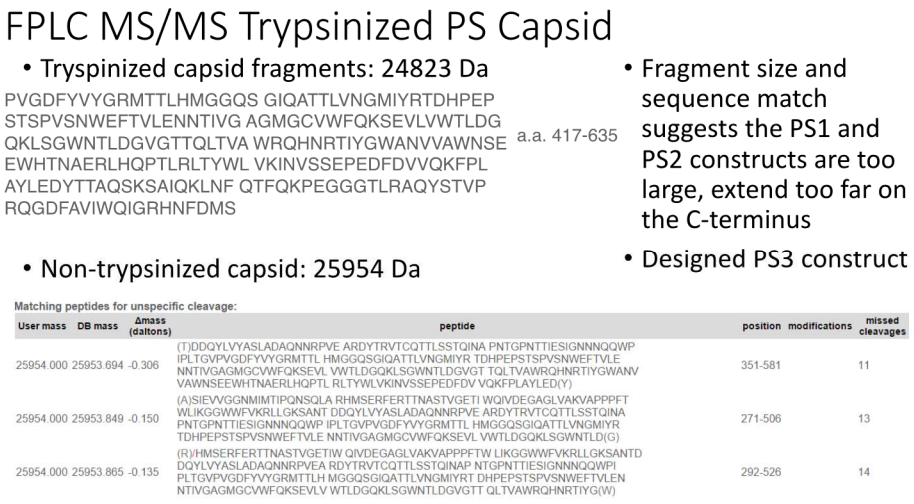

Figure XXXII. FPLC MS/MS of trypsinized capsid fragments after gel extraction.

Intact mass of the ~25 kDa band after gel extraction is 25,954 Da

Table 4. Human astrovirus PS spike construct boundaries, plasmids and expression system.

List of PS spike constructs residues and tags and expression systems used to express the constructs.

Plasmid	Description
pHisGB1_PS1	Residues: 394-655; moderate expression, ~1 mg/L, largely insoluble, degraded
pHisGB1_PS2	Residues: 394-737; Moderate expression, ~1 mg/L, mostly insoluble, degraded
pHisGB1 PS3	Residues: 394-615; Moderate expression, ~1 mg/L, mostly insoluble, degraded
pET52b PS1	Residues: 394-655; 6xHis tagged, poor expression <0.5mg/L, insoluble
pET52b PS2	Residues: 394-737; 6xHis tagged, poor expression <0.5mg/L, insoluble
pGEX PS1	Residues: 394-655; Moderate expression, ~1-2 mg/L, low purity after GST purification, degraded
pGEX PS2	Residues: 394-737; Moderate expression, ~1-2 mg/L, low purity after GST purification, degraded
pHisGB1 PS4	Residues: 394-660; Modest expression, ~1 mg/L, low purity after TALON, degraded
pHisGB1 PS5	Residues: 394-653; Modest expression, ~1 mg/L, low purity after TALON, degraded, mostly insolubly expressed
pHisGB1 PS6	Residues: 417-645; Modest expression, ~1 mg/L, low purity after TALON, degraded, mostly insolubly expressed
pHisGB1 PS7	Was not cloned successfully
pHisGB1 PS8	Residues: 394-645; Modest expression, ~1 mg/L, low purity after TALON, degraded, mostly insolubly expressed
pHisGB1 PS9	Residues: 433-678; Modest expression, ~1 mg/L, low purity after TALON, degraded, mostly insolubly expressed
pHisGB1 PS10	Residues: 417-640; Modest expression, ~1 mg/L, low purity after TALON, degraded, mostly insolubly expressed
pfastBac PS11	Residues: 417-689; Expressed poorly in Sf9 cells

	with N-terminal 6xHis, <0.5 mg/L, no expression (soluble or insoluble)
pFastBac PS12	Residues: 417-678; Expressed poorly in Sf9 cells with N-terminal 6xHis, <0.5 mg/L, no expression (soluble or insoluble)
pFastBac PS4	Residues: 394-660; Expressed poorly in Sf9 cells with N-terminal 6xHis, <0.5 mg/L, no expression (soluble or insoluble)

Appendix III

Engineering pre-fusion form stabilized HPIV3 Fusion protein

The project goal is to engineer the HPIV3 F protein in its pre-fusion form, and characterize the protein by structural, biophysical, and immunogenic studies. We propose a novel mutagenesis strategy that stabilizes recombinant F protein ectodomain in the pre-fusion form by replacing the inherently unstable residues in the trimeric coiled HRB region with 'ideal' residues (Ile) which form optimal hydrogen bonding and hydrophobic packing interactions along the length of the stalk Figure XXXIV). We hypothesize that our engineering strategy will allow structural and biophysical characterization of the F protein that will advance our understanding of protein- mediated membrane fusion, a mechanism fundamental to all enveloped viruses. We also hypothesize that our engineering strategy will yield a highly immunogenic pre-fusion F protein that will elicit a protective neutralizing antibody response in the cotton rat model. Furthermore, we hypothesize that the engineering strategy will be broadly applicable to related Fusion proteins such as Measles, Mumps and Hendra virus and will facilitate structural and antigenic studies on the pre-fusion F. Thus, our studies will advance understanding of paramyxovirus entry into human cells, and provide preliminary immunogenicity studies to validate the use of pre-fusion HPIV3 F protein as a vaccine candidate.

By using the heptad repeat trimeric coiled coil idealization strategy isoleucines were placed at the a and d position (Figure XXXIV). The constructs and

expression systems are summarized in Table 5. The rationale for the constructs and mutations is summarized in Table 6. Yields did not scale up from small scale insect expression (Figure XXXVI). Observed multiple contanimants after strep purification (Figure XXXVI). Number of expression optimizations did not improve yieild or purity. Decided to consider alternative expression systems, such as mamallian cells. Expression in 293 had low yields (overall much better than S2 cells, ~0.5 mg/L) and purity was much higher than that from insect cells expressions (Figure XXXVII). Expressed HPIV3 F in Sf9 cells, 293 cells and Expi293 cells (Figure XXXV and Figure XXXVI). All constructs and expression systems had low yields, <0.5 mg/ml (Figure XXXVII, Figure XXXVIII, Figure XXXIX). Electron microscopy of HPIV3 F1 construct with idealized coiled coil purified from transiently transfected 293 cells did not produce clear, consistent particles (Figure XL). HPIV3 F protein was purified on sizing and performed SAXS and observed aggregation (Figure XLI). For future directions, consider combining mutants, using stably transfected mammalian cells and using antibodies to stabilize prefusion conformation.

Table 5. HPIV3 F protein list of plasmids and construct descriptions (and RSV F constructs).

Plasmid	Description
HPIV3 F wt insert in pUC57-Kan.seq	HPIV3 F wt in pUC57 for cloning
pMT_Bip_HPIV3_F_R106Q,S164P,HRBIdealized	HPIV3 F with R106Q, S164P, and HRB Idealized
pMT_Bip_HPIV3_F2_R106Q_HRBIdealized	HPIV3 F with R106Q, and HRB Idealized
pMT_Bip_HPIV3_F3_HRBIdealized	HPIV3 F HRB Idealized
pMT_Bip_HPIV3_F4_wt	HPIV3 F wild type
pMT_Bip_HPIV3_F4_wt_GCNt	HPIV3 F with GCNt trimerization domain
pcDNA3.1(+)_HPIV3_F2_R106Q_TPA_ss	HPIV3 F R106Q TPA secretion signal
pcDNA3.1(+)_HPIV3_F2_R106Q_WT_ss	HPIV3 F R106Q wt HPIV3 secretion signal
pCF_Intron_HPIV3_F_R109_GCNt_CO_TPA	HPIV3 F R109 GCNt domain codon optimized for mammalian expression, TPA secretion signal
pCF_Intron_HPIV3_F1_TPA_ss_Gibson	HPIV3 F with R106Q, S164P, and HRB Idealized, mammalian expression optimized, TPA secretion signal
pCF_Intron_HPIV3_F2_TPA_ss	HPIV3 F with R106Q, and HRB Idealized, mammalian expression optimized, TPA secretion signal
pCF_Intron_HPIV3_F3_TPA_ss	HPIV3 F HRB Idealized, mammalian expression optimized, TPA secretion signal
pCF_Intron_HPIV3_F4_TPA_ss_Gibson	HPIV3 F wild type, mammalian expression optimized, TPA secretion signal
pCF_Intron_HPIV3_F4wt_TPA_ss_GCNt_10xHis	HPIV3 F wild type with GCNt trimerization domain and C-terminal 10xHis tag, mammalian expression optimized, TPA secretion signal
pLEXm_RSV_F_DS-Cav1_Annotated	RSV F DS-Cav1 from McLellan lab
pLEXm_RSV_F_sc9-10_DS-Cav1	RSV F sc9-10 construct
pCF_RSV_F_Ile_TPA_ss_muta	RSV F with idealized HRB, and TPA secretion signal in pCF plasmid (originally from pLEXm)

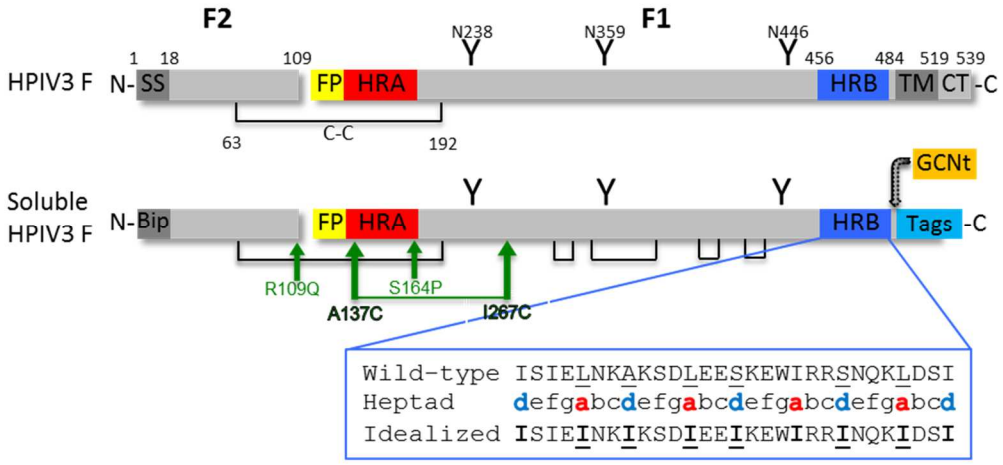

Figure XXXIII. HPIV3 F idealization strategy.

Mutanting every d and a position of the heptad coiled coil to isoleucine to increase stabilizing interactions.

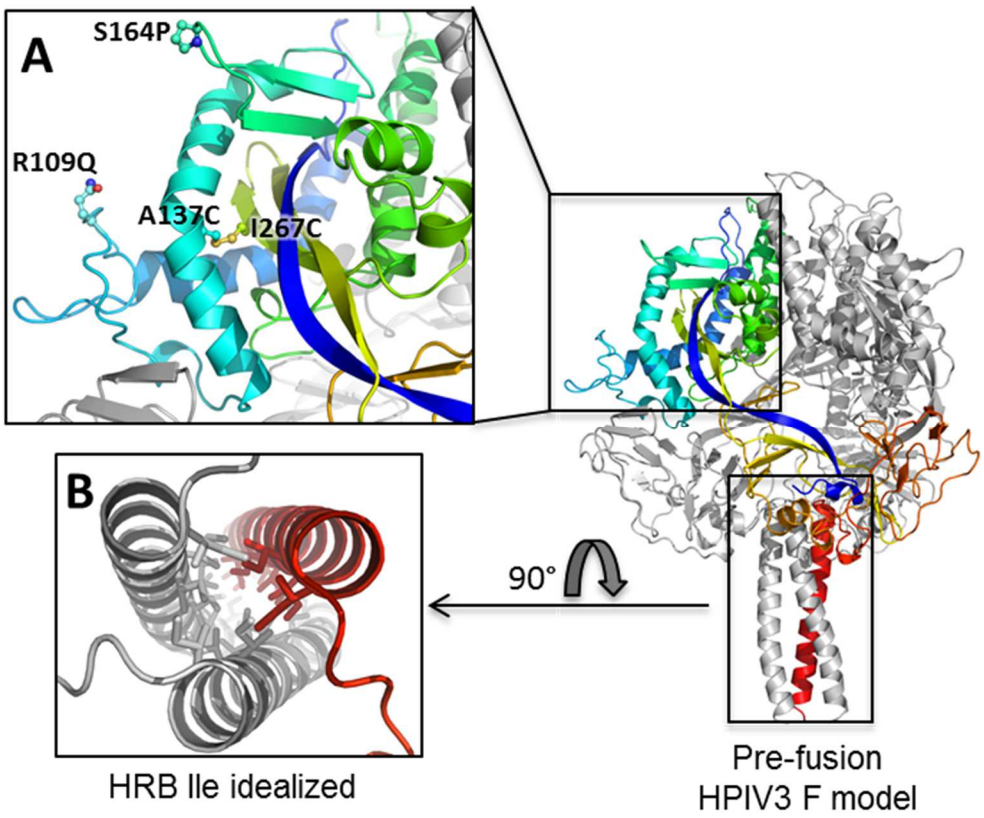

Figure XXXIV.HPIV3 F HRB Ile idealization strategy model and additional

stabilizing mutations.

A. Mutations S164P: stabilize turn of β-strands 5 and 6 in HRA, prevents spring-loaded function during triggering, R109Q: cleavage inactive, prevents exposed fusion peptide, A137C, I267C: β–carbons are 4-5 Å apart in pre-fusion HPIV3 F model and over 110 Å apart in the post-fusion HPIV3 F crystal structure. B. View down HRB isoleucine idealized coiled coil.

Table 6. List of HPIV3 constructs and the role of the mutations.

Construct	Mutations	Rationale
F_{GCNt}	C-terminal GCNt isoleucine zipper	Pre-fusion control
F_1	Idealized HRB, R109Q, S164P	Pre-fusion, cleavage inactive, β-turn stabilized
F_2	Idealized HRB, R109Q	Pre-fusion, cleavage inactive
F_3	Idealized HRB	Pre-fusion, cleavable
F_4	Idealized HRB, A137C and I267C	Pre-fusion, cleavable, disulfide linking α2 with β6
F_{wt}	None	Post-fusion control

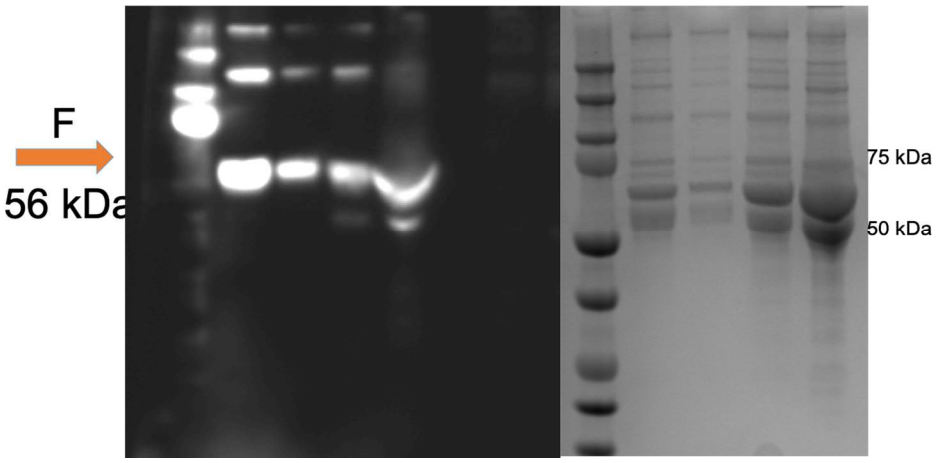

Figure XXXV. Small scale expression in stably transfected S2 cells.

HPIV3 F constructs expressed in ug quantities. Purified via strep and TALON. After tandem purification, a major contaminant BSA remained.

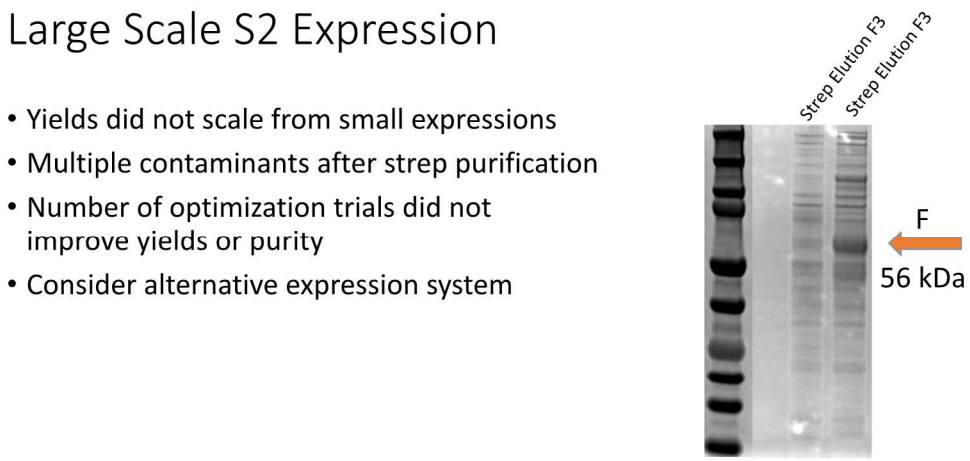

Figure XXXVI. Large scale S2 expression of HPIV3 F constructs.

Yields were low microgram quanitties and purity was low with a number of contaminants.

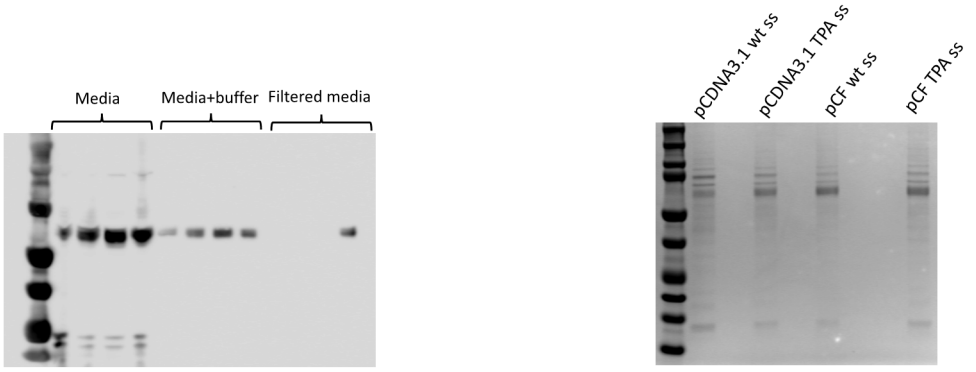

Figure XXXVII. Small scale expression of HPIV3 F constructs in 293 cells using transient transfection.

pCDNA and pCF plasmids with wild type secretion HPIV3 signal sequence or TPA secretion signal were used.

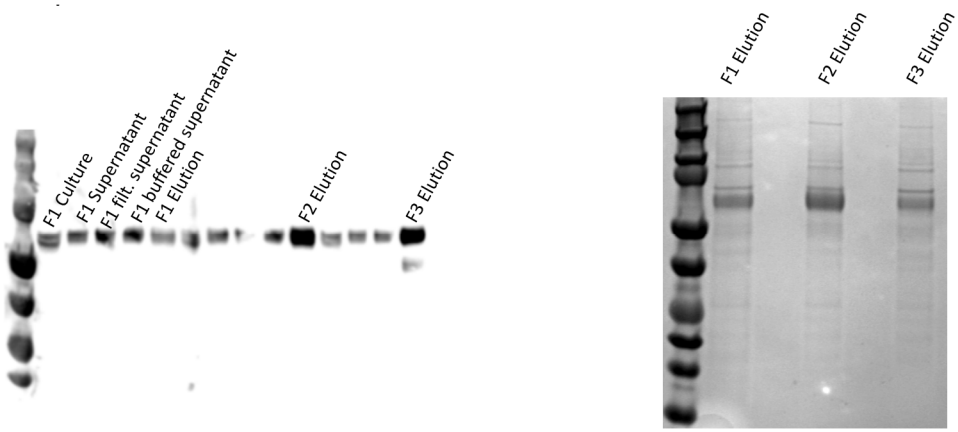

Figure XXXVIII. Expression of HPIV3 F protein constructs in 293 cells.

TALON batch purification and representative gel showing purity of HPIV3 F constructs

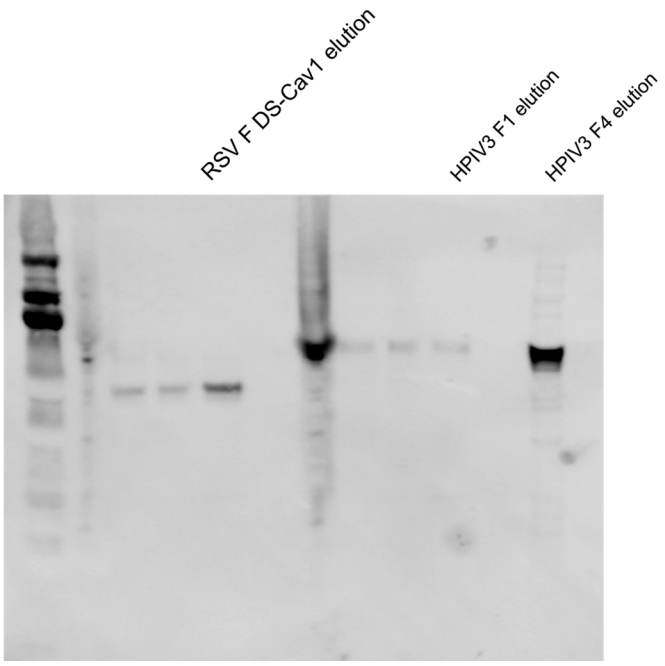

Figure XXXIX. Expi293 expression and purification of RSV F dsCav1 and HPIV3 F constructs.

After purification and quantification, yields were ~<0.5mg/ml.

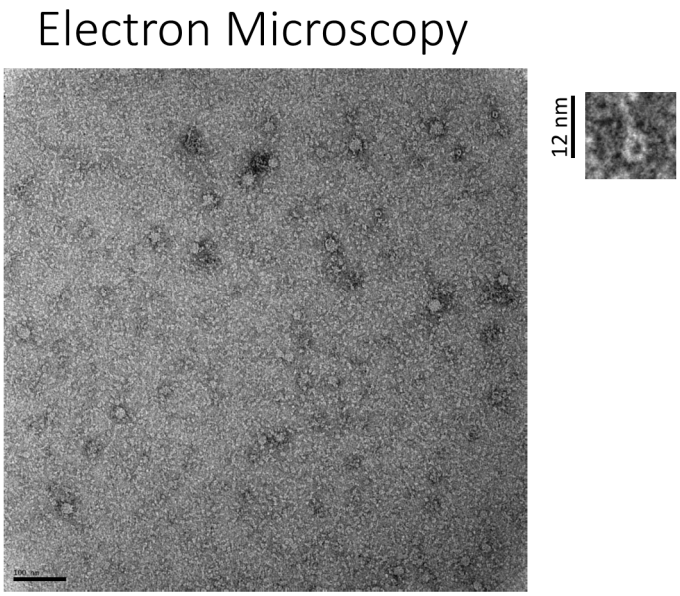

Figure XL. Electron microscopy of HPIV3 F coiled coil idealizied construct.

EM Image is incoclusive, with no distinct patter or consistent particles sizes or conformation.

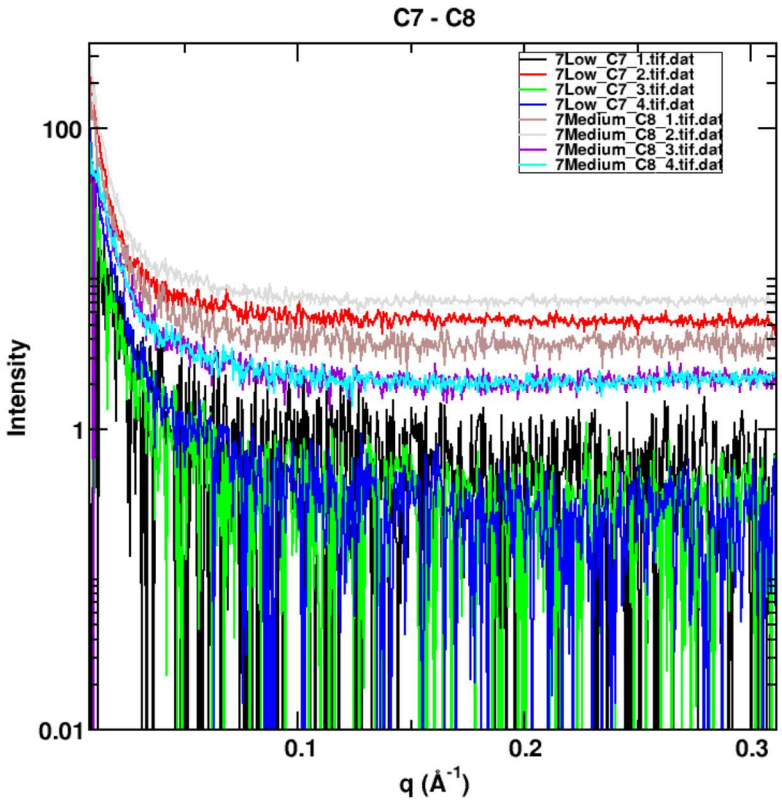

Figure XLI. Small angle X-ray scattering of HPIV3 F1.

The plot is indicative of an aggregated protein. Aggregates have high intensity relative to folded protein and thus can mask signal from folded protein.

Appendix IV

RSV G and Trellis mAbs

Table 7. RSV G plasmids and construct descriptions.

Plasmid	Description
pMT_Bip_RSV_G_148_197	RSV G 148-197
pMT_Bip_RSV_G_161_197	RSV G 161-197
pMT_Bip_RSV_G_162_188	RSV G 162-188
pMT_Bip_RSV_G_164_194	RSV G 164-194
pMT_Bip_RSV_G_ecto_no_his	RSV G ecto 64-298, strep tag only
pMT_Bip_RSV_G_Full	RSV G ecto 64-298, his tag and strep tag
pRSFDuet_PelB_RSV G 148-197 5_31_18	RSV G 148-197 with C-terminal 6xHis tag in pRSF_Duet plasmid
pRSFDuet-RSV G 157-197 + CX3CR1 N term extended	RSV G 157-197 in first MCS and CX3CR1 N-terminal peptide res. 3-24 in second MCS
pRSFDuet-pelB RSV G 157-197 pelB 1G8 scFv	RSV G 157-197 in first MCS and 1G8 N-scFv in second MCS
pRSFDuet-RSV G 157-197	RSV G 157-197 with C-terminal 6xHis tag in pRSF_Duet plasmid
pRSFDuet-pelB RSV G 148-197 mutagenesis	Deleted first start codon with MCS in frame (this improved expression)

pET52b_RSV_G_164-194_Gibson	RSV G 164-197, C-terminal 6xHis tag
pET52b_RSV_G_162-188_Gibson	RSV G 162-188, C-terminal 6xHis tag
pET52b_RSV_G_161-197	RSV G 161-197, C-terminal 6xHis tag
pET52b_RSV_G_161-197+strep	RSV G 161-197, C-terminal strep tag
pET52b_RSV_G 148-197_F160A_N161A_3_8_17	RSV G 148-197, F160A N161A C-terminal 6xHis tag
pET52b_RSV_G 148-197_F168A_N169A_3_8_17	RSV G 148-197, F168A N169A C-terminal 6xHis tag
pET20b RSV G 157-197	RSV G 157-197 with pelB secretion signal
pET52b RSV G 148-197	148-197 6xHis tag
pET52b RSV G 157-197	157-197 6xHis tag
pET52b_RSV_G 148-197 strep	148-197 6xHis and strep tag

Table 8. Trellis mAb suite constructs and plasmids

pMT_puro_bip_2xStrep_3G12.strpMT_puro_bip_2D10.str

Plasmid	Description
pET-52b(+)-3D3	3D3 scFv 6xHis
pET20b_3D3_scFv	3D3 scFv pelB ss, 6xHis
pMT_3D3_scFv	3D3 scFv Bip ss, 6xHis, Strep tag
pMT_puro_bip_3G12	3G12 scFv, Bip ss, puro resistance, 6xHis, 2xStrep
pMT_puro_bip_3D3	3D3 scFv, Bip ss, puro resistance, 6xHis, 2xStrep
pMT_puro_bip_2D10	2D10 scFv, Bip ss, puro resistance, 6xHis, 2xStrep
pMT-puro-bip 6A12scFV	6A12 scFv, Bip ss, puro resistance, 2xStrep
pMT-puro-bip 1G1scFV	1G1 scFv, Bip ss, puro resistance, 6xHis, 2xStrep
pMT-puro-bip 2B11scFV	2B11 scFv, Bip ss, puro resistance, 6xHis, 2xStrep
pMT_puro_bip_2xStrep	Empty pMT puro plasmid, 2xStrep
pMT_puro_bip_2xStrep_2D10.str	2D10 scFv, Bip ss, puro resistance, 2xStrep
pMT_puro_bip_2xStrep_3D3	3D3 scFv, Bip ss, puro resistance, 2xStrep
pMT_puro_bip_2xStrep_3G12.str	3G12 scFv, Bip ss, puro resistance, 2xStrep
pET52b RSV G 1G8_scFv_2_22_18	1G8 6xHis tag
pET52b RSV G 2B11_scFv_2_22_18	2B11 6xHis tag
pMT-puro-bip 2B11scFV	pMT puromycin selection, 2B11 scFv
pCMV_mAb 1G1 heavy	1G1 heavy chain variable domain in VRC01 Mab heavy chain
pCMV_mAb 1G1 Light	1G1 light chain variable domain in VRC01 Mab light chain
pCMV_mAb 1G8 heavy	1G8 heavy chain variable domain in VRC01 Mab heavy chain
pCMV_mAb 1G8 VRC01 Light Chain CMV_R	1G8 light chain variable domain in VRC01 Mab light chain
pCMV_mAb 2B11 heavy	2B11 heavy chain variable domain in VRC01 Mab heavy chain
pCMV_mAb 2B11 Light	2B11 light chain variable domain in VRC01 Mab light chain
pCMV_mAb 6A12 heavy	6A12 heavy chain variable domain in VRC01 Mab heavy chain
pCMV_mAb 6A12 Light	6A12 light chain variable domain in

	VRC01 Mab light chain
pCMV_mAb 2D10 light	2D10 light chain variable domain in VRC01 Mab light chain
pCMV_mAb 2D10 heavy	2D10 heavy chain variable domain in VRC01 Mab heavy chain
pCMV_mAb 3D3 light	3D3 light chain variable domain in VRC01 Mab light chain
pCMV_mAb 3D3 heavy	3D3 heavy chain variable domain in VRC01 Mab heavy chain
pCMV_mAb 3G12 heavy	3G12 heavy chain variable domain in VRC01 Mab heavy chain
pCMV_mAb 3G12 light	3G12 light chain variable domain in VRC01 Mab light chain